PAPER

Check for updates

Natural gum-modified mucin nanocarriers with enhanced mucoadhesion and *trans*-cornea infiltration for controlled drug delivery in ocular uveitis therapy

Wahida Binte Naz Aurthy, [ID] [a] Nondita Datta,[a] Siew Yee Wong, [ID] [b] Xu Li, [ID] [bc] Asma Rahman,[d] Md. Latiful Bari, [ID] [d] Ishtiaque Anwar[e] and M. Tarik Arafat [ID] *[a]

Ocular uveitis is a major health concern due to the limited efficacy of current antibiotic eye drops. Conventional treatments require frequent reapplication as they have low bioavailability and show slow drug action at the infection site. To address this, a novel eye drop formulation was developed using mucin-based nanoparticles (Mu NPs) that encapsulate ciprofloxacin. In the ionic gelation technique, the COO^- groups of the mucin chain interacted electrostatically with cationic crosslinkers to form NPs, and then, Mu NPs were stabilized using xanthan gum for extended shelf life. TEM and DLS studies confirmed variations in particle size and surface charge based on the crosslinker concentration. *In vitro*, *ex vivo*, and *in vivo* biocompatibility tests showed excellent safety, including <4% hemolysis ratio, and the Draize test also confirmed the biocompatibility. The formulation had 95% drug encapsulation efficiency and controlled drug release rate with 40–50% release in the first 8 hours. In rabbit eye models, induced inflammation and bacterial infection were treated successfully within 3 and 7 days, respectively. The histopathological analysis of infected corneas proved the completion of internal healing. The high mucoadhesiveness of mucin enhanced drug retention in the aqueous humor (0.26 µg mL^{-1}) even after 8 hours, outperforming commercial eyedrops. These findings suggest mucin NPs as a promising mucoadhesive drug delivery system for infectious and inflammatory eye diseases.

1. Introduction

Ocular infection and inflammation are commonly treated with topical and systemic drugs. However, this therapeutic approach may have limitations in terms of penetration, concentration, and frequency. In order to avoid irreparable vision loss, bacterial uveitis must be diagnosed and treated as soon as possible.[1] Bacterial infection and the human immunological response are among the primary causes of inflammation, with symptoms including visual discomfort, photophobia, impaired vision, and redness affecting the uveal tract including the iris, choroid and ciliary body.[2,3] Infectious uveitis remains a clinically significant cause of visual morbidity globally, affecting both the anterior and posterior parts of the eye.[4] If left untreated, it can lead to scarring, glaucoma, retinal detachment, and cataracts, as well as post-operative problems.[5–7] Gram-positive cocci, particularly *Staphylococcus aureus*, and coagulase-negative staphylococci, specifically *S. epidermis*, are among the most frequently isolated pathogens in both keratitis and intraocular infections.[8]

The delivery of drugs to the eye for alleviating ocular issues is complicated because there are several ocular barriers and layers that limit drug availability (<10%) in the affected tissues.[9–11] Conventional treatment approaches face further challenges due to rapid blinking and nasolacrimal drainage. Thus, there is a potential demand for drug delivery vehicles. Bioavailability can be improved by using viscosity-enhancing agents and mucoadhesive polymers as drug carriers to prolong retention on ocular tissues, reducing the need for frequent administration. Recent studies have reported the use of surface roughness-controlled dual drug-loaded ceria nanocarriers for treating ocular chemical burns and polycaprolactone-based nanoparticles for managing macular degeneration by solving common ocular challenges, demonstrating the potential of nanomedicine strategies for targeting both anterior and posterior segment diseases.[12,13]

[a] Department of Biomedical Engineering, Bangladesh University of Engineering and Technology (BUET), Dhaka-1205, Bangladesh. E-mail: tarikarafat@bme.buet.ac.bd
[b] Institute of Materials Research and Engineering (IMRE), A*STAR (Agency for Science, Technology and Research), Singapore 138634, Singapore
[c] Institute of Sustainability for Chemicals, Energy and Environment (ISCEE), A*STAR (Agency for Science, Technology and Research), Singapore 138634, Singapore
[d] Center for Advanced Research in Sciences (CARS), University of Dhaka, Dhaka 1000, Bangladesh
[e] Bangladesh Eye Hospital, Dhanmondi, Dhaka 1205, Bangladesh

Nanocarrier-based systems, for example, niosomes, liposomes, polymeric and metallic nanoparticles, and nanogels, have been explored to extend the retention duration and boost the ocular availability of loaded drugs.[14–19] Carbon dots also show less toxicity and improved ocular retention than carbon nanotubes or graphene oxide.[20] The chemical instability, hydrolysis, or oxidation of the unsaturated lipid that makes up liposomes restricts their application in drug administration by allowing the encapsulated medicine to leak before it reaches its target site.[21]

Ocular mucins are present in tear films, which is crucial for preserving the balance of the wet corneal surface, trapping allergens and promoting their elimination, as well as contributing to the lubrication of ocular surfaces and maintaining the integrity of the mucosal barrier.[22,23] Mucoadhesion is the phenomenon where two materials, one of which is a mucosa, remain connected to each other due to interfacial forces.[24] Mucin-associated mucoadhesive delivery techniques are advantageous as they adhere to the mucous membrane layer, which prolongs drug or bioactive molecule retention.[25,26] Mucin has been used as a coating for the protection of other drug carriers.[27,28] The functional features of mucin make it a suitable carrier for sustained ophthalmologic drug delivery. Blocking the spreading and anchoring of inflammatory cells to the eye by mucin is one method of treating ocular infection as well as inflammation. According to studies, MUC5AC can capture allergens, debris, and pathogens to help remove them from mucosal surfaces.[29] Membrane-bound mucin on the apical surface of corneal epithelium, acting as a selective barrier, forms a protective glycocalyx and gives protection from pathogens.[30]

Despite all the beneficial roles of mucin, it is yet to be explored as a standalone mucoadhesive nanocarrier in ophthalmology. Mucin nanoparticles have recently been developed by DNA and UV crosslinking, which increases the formulation complexity and limits scalability.[31] The development of mucin nanoparticles using a simple one-step ionic gelation process for ocular drug delivery applications to improve bioavailability has not yet been documented in any research.

The inclusion of glycerin, xanthan gum, and mucin in the formulation is motivated by their supporting qualities that increase the therapeutic value of ocular drug delivery systems. Glycerin is an ophthalmic demulcent that forms a soothing film on the mucous membrane surfaces of the eye and has intraocular pressure (IOP)-reducing characteristics.[32] Its anti-irritant and anti-inflammatory properties provide temporary relief from discomfort.[33,34] Xanthan gum, processed from fermenting *Xanthomonas campestris*, is a natural and fully biodegradable polymer and has the capacity to improve mucoadhesion. It is a common agent in the pharmaceutical industry to enhance the retention time of the drug and increase its therapeutic activity at the target site. The mucoadhesive property of this gum plays an important role of holding the nanocarrier attached to the biological site by interfacial force and provides extended release of the desired drugs.[35,36] The properties of glycerin, xanthan gum and mucin make them appropriate for ophthalmic usage.

Compared to other polymeric nanoparticle production methods, ionotropic gelation is one of the least expensive and simple techniques to produce nano or macro particles.[37] When a drug or bioactive molecule is added to the process, it can be entrapped within the polymeric chains and become trapped inside the nanoparticle/microparticle structure.[38] Various crosslinking methods have been introduced for negatively charged polymers similar to mucin such as alginate.[39,40] In the case of crosslinking mucins, thiol-based crosslinkers are used.[41] Using bivalent cations as crosslinking agents combines the carboxylic group of glycan cores, and thus sialic acid groups become occupied in the synthesis process.

This study aims to synthesize and characterize mucin nanoparticles, which have been studied hardly to this date. It focuses on developing nanoparticles using the ionic gelation technique and evaluating their physicochemical properties by varying crosslinker type (cations, polymers, and gums) as well as concentration for ocular drug delivery applications. Ciprofloxacin was selected as a model antibacterial drug to fight bacterial uveitis. The application of the nanoparticles in the incorporation of an antibiotic drug, ciprofloxacin, into a nanoparticle-based delivery system was described along with the drug release profile with respect to time. *In vitro*, *ex vivo* and *in vivo* tests, for instance, hemolysis and corneal histology tests, and the Draize test were performed to ensure the biocompatibility of the formulation. The therapeutic efficacy and ocular retention of the mucin nanoparticles were further assessed using a rabbit model of ocular infection and inflammation.

2. Materials and methods

2.1. Materials

Mucin from porcine stomach (Type II, M_w = 640 000 g mol^{-1}, bound sialic acid, $\leq$1.2%, solubility 1 M NaOH: soluble 20 mg mL^{-1}), which served as the primary polymer for nanoparticle synthesis, was purchased from Sigma-Aldrich. Chitosan (source: shrimp shells; degree of deacetylation $\geq$75%) was also obtained from Sigma-Aldrich. The other chemicals used in the NP synthesis are as follows: calcium chloride and xanthan gum were purchased from Research Lab, glycerol from Emplura®, the drug ciprofloxacin lactate (CIP) from Incepta Pharmaceuticals. CIP's pharmacokinetic characteristics and widespread clinical use make it a key indicator for innovative delivery systems designed to treat ocular bacterial inflammation and infection. Sodium chloride (NaCl), potassium chloride (KCl), potassium phosphate (KH_2PO_4), ethanol (C_2H_5OH), and sodium hydrogen phosphate (Na_2HPO_4) were purchased from Merck, Germany. Both nutrient broth and nutrient agar were obtained from HiMedia, India. All reagents were of analytical grade.

2.2. Synthesis of mucin NPs

Mucin nanoparticles (Mu NPs) were synthesized through the ionic gelation technique in a neutral pH medium, dispersed in distilled water. Ionic gelation is a process that allows the synthesis of nanoparticles and microparticles by electrostatic interactions

between two ionic species under appropriate conditions. A polymer must be present in at least one of the species. This method is selected for synthesis due to its simplicity and affordability along with the lack of complex machinery and short processing time.[42] Briefly, 0.2 g mucin powder was dissolved in 20 mL deionized (DI) water to form 1% w/v dispersion. The dispersion was stirred for 30 min until it became completely homogeneous. Separately, 0.04 g $CaCl_2$ was dissolved in 4 mL DI water to prepare the crosslinking solution and this solution was added to the dispersion dropwise with the help of a 23G syringe at a controlled rate to ensure uniform ionic crosslinking. Sonication was performed to eliminate any possible cluster of NPs. The sample was kept under stirring for 4 h. Fig. 1 presents the overview of bonding behind the crosslinking process. Nanoparticles were produced using the same technique while varying the crosslinker concentration and type. In a different formulation, instead of cationic crosslinkers, positively charged chitosan (CS) and guar gum (GG) were also used in the crosslinking process. The concentration of both the polymer and the crosslinker has been varied to observe the change in the properties of NPs. In order to modify the synthesis process with gums or glycerol, 0.5% xanthan gum or 10% glycerol was first dissolved and then a mucin dispersion was formed in the same solution and after that the crosslinking step was done, and finally, xanthan gum-based mucin NP (Mu-XG) and glycerol-based mucin NP (Mu-Gly) were synthesized.

2.3. Drug-loaded Mu NP synthesis

First, 0.3% w/v CIP was added to the crosslinker solution. Then, the mixture of crosslinker and drug was kept under stirring for 5 min and then added dropwise to the mucin dispersion according to the same procedure discussed in the previous paragraph. The NP formulation incorporated with the drug was centrifuged to obtain solid NPs, and then it was freeze-dried for

attenuated total reflectance-Fourier transform infrared (ATR-FTIR) spectroscopy and for measuring the drug loading capacity.

2.4. Zeta potential and polydispersity index

Zeta potential (ZP), also known as the surface charge, is the difference in charge between the surface of the particle and the stern layer. To measure the ZP and particle size distribution of NPs, a dynamic light scattering (DLS) technique was used with a Zetasizer. DLS was used to characterize the hydrodynamic diameter of the nanoparticle formulations. ZP measurements were made with the same instrument *via* electrophoretic mobility. The electrophoretic mobility of the NPs in aqueous suspensions was used for zeta potential determinations.

2.5. Transmission electron microscopy (TEM)

TEM (JEOL 2100) was used to investigate the morphological properties of the NPs and particle size distribution. NPs were dispersed in ethanol, sonicated for 20 min, and then poured onto the TEM grid for the test.

2.6. ATR-FTIR spectroscopy

To study the chemical bonds formed in the mucin polymer structure, the ATR-FTIR spectra of the samples were recorded in the range of 4000–700 cm^{-1} using a Nicolet iS5 FTIR Spectrometer (Nicolet Instrument Corporation, WI, USA).

2.7. Quantification of the drug loading capacity and drug entrapment efficiency

The nanoparticle samples were prepared with and without drug. Both samples were then centrifuged for 30 min at 9000 rpm. Then the supernatant was removed, and the collected NP was freeze dried. The weight of both of the dry
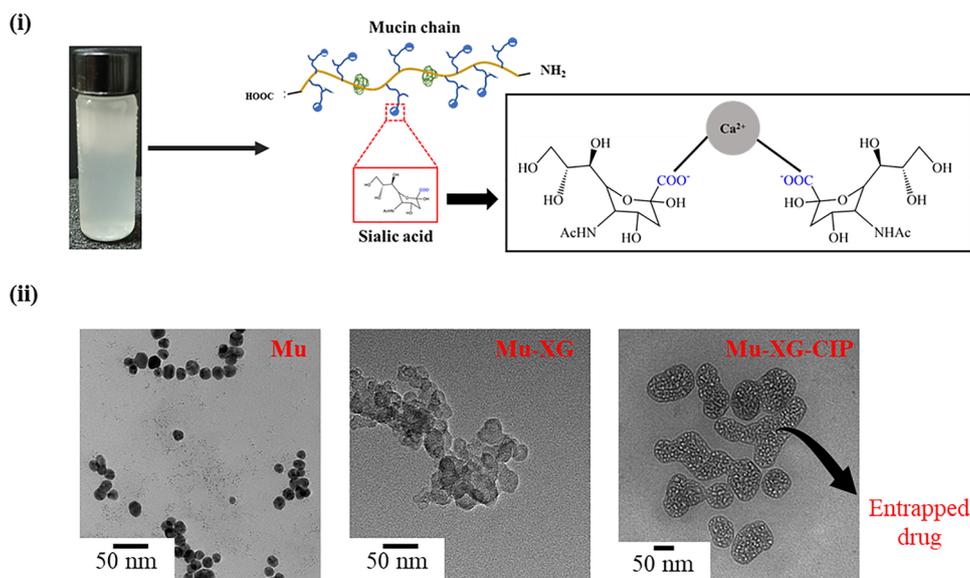

Fig. 1 Crosslinking mechanism behind the nanoparticle formation and TEM images of particles. (i) The COO^- group present in the sialic acid plays a major role in forming linkage among chains using Ca^{2+} ions. (ii) Mu-XG NP has a whitish zone surrounding the outer surface, showing the presence of xanthan gum, and after the incorporation of ciprofloxacin, a granular structure is seen in MuXG–CIP NP.

samples, with and without drug, was measured. The loading capacity (%DLC) was calculated using the following equation:

$$\%DLC = \frac{W_d - W_p}{W_d} \times 100\%$$

where W_d is the mass of drug-loaded NP and W_p is the mass of the pure NP without drug.

To measure the drug entrapment efficiency (%DEE) of mucin NPs, the previously formed dispersion was centrifuged (Nüve) at 9000 rpm for 40 min, and the drug content was assessed in the supernatant. The CIP concentration was measured using a UV-vis spectrophotometer (Shimadzu UV-3100) at 275 nm and determined using a previously constructed calibration curve. The entrapment efficiency was calculated using the following equation:

$$\%DEE = \frac{W_T - W_S}{W_T} \times 100$$

where W_T is the total mass of drug present in the sample and W_S is the drug mass in the supernatant.

All experiments were conducted in at least triplicate. Unless otherwise stated, the results are presented as mean $\pm$ standard deviation, and Student's t-test analysis was performed, followed by ANOVA test. $*p < 0.05$ was considered statistically significant. $**p < 0.01$ and $***p < 0.001$ were considered highly statistically significant.

2.8. *In vitro* drug release study

The release study was performed in a phosphate buffer saline (PBS, pH 7.4) for 48 h. At predetermined time points (0.16, 0.5, 1, 2, 3, 4, 5, 6, 7, 8, 24, 26 and 30 h), aliquots (4 mL) were withdrawn at different time intervals to determine the drug concentrations, and in all cases, the sample was returned to maintain the constant volume. A dialysis membrane of 14 kDa pore size was used to confine the polymeric fragments, allowing only dissolved drug to diffuse into the release medium. This method prevents any possible inaccuracy due to burst leakage or noise in the spectroscopy. Moreover, the membrane mimics the physiological barrier. The formulation-loaded dialysis bag was securely sealed from both ends of the membrane to prevent leakage of the formulation and was kept at 37 °C in a shaker incubator at a speed of 100 rpm to replicate the *in vivo* environment, submerged in 100 mL PBS. The concentration of CIP was determined using a UV-vis spectrophotometer at 275 nm.

Cumulative drug release (%)

$$= \frac{\text{Amount of CIP in the release medium}}{\text{Initial amount of CIP loaded on NP}} \times 100\%$$

2.9. Antibacterial property test by a well diffusion method

Nanoparticles with and without antibiotic (negative control) were prepared for the well diffusion test. *Staphylococcus aureus*, typical representative of Gram-positive bacteria, was used in the assay, and bacteria were cultured overnight in nutrient broth. Then, 100 μL bacterial solution from the broth was spread into the agar plates. After that, 30 μL of CIP-loaded Mu NP solution was poured into the well to observe the inhibition zone. The plates were incubated at 37 °C for 24 h. The diameters of the inhibition zones were measured after this time. This test was compared to the commercially available ciprofloxacin eye drop as well.

2.10. *In vitro* hemolysis test

A hemolysis assay was performed according to a previously published protocol.[43,44] The blood was stored in citrate tubes to prevent clotting. The RBCs were collected by centrifugation at 1500 rpm for 15 min. Then, a solution was prepared by adding 1 mL of centrifuged erythrocytes into 49 mL of PBS. The nanoparticle dispersions were prepared in PBS. Then 10 mL of stock solution was added to 1 mL of the nanoparticle sample. The solutions were mixed and incubated for 1 h at 37 °C in an incubator. The percentage of hemolysis was measured by UV-vis spectrophotometry analysis of the supernatant at 545 nm absorbance after centrifugation at 2000 rpm for 15 min. Here, 1 mL of PBS was used as the negative control and 1 mL of Triton X-100 was used as the positive control. All hemolysis data points were presented as the percentage of the complete hemolysis.

$$\%\text{Hemolysis} = \frac{[A]_{\text{test}} - [A]_{\text{neg}}}{[A]_{\text{pos}} - [A]_{\text{neg}}} \times 100\%$$

where $[A]_{\text{test}}$, $[A]_{\text{pos}}$, and $[A]_{\text{neg}}$ are the absorbance values of sample, positive and negative control, respectively.

2.11. *Ex vivo* mucoadhesion test

Mucoadhesion test was performed using excised goat eyes to evaluate how much of the applied sample adheres to the ocular epithelial surface according to a previously published study on a polymeric drug carrier.[37] A falling liquid film test was used to measure the adhesion strength of the nanoparticle sample. The solution of mucin NP penetrated through the ocular layer, and thus, the amount of adsorbed sample with respect to the applied amount was calculated. The sample was poured onto ocular surface dropwise at a slow pace allowing the liquid to fall. The non-adhered sample was collected from the petri dish placed beneath the eye. The applied amount (W_a) was measured and then the lost amount (W_l) which had fallen from the surface was measured. The percentage of adsorbed amount was calculated using the following equation:

$$\%\text{Mucoadhesion} = \frac{W_a - W_l}{W_a} \times 100\%$$

2.12. Molecular docking study

The interaction type between the polymeric mucin chain and the mucin present in the ocular surface has to be identified. The mucoadhesion due to hydrogen bonds was investigated *in silico* using the AutoDockTools software. Mucin structures (MUC1 as ocular mucin and MUC2 as polymeric mucin) were downloaded from the RCSB Protein Data Bank in the PDB format. First, protein preparation was carried out to optimize the protein structure and improve precision in docking simulations.[45,46] Water molecules are removed to simplify the protein structure and to accurately model the protein's behavior during docking

simulations. This structure was completed by adding Kollman charges to get more accurate and specific docking predictions. The Kollman charges are considered to be more accurate than Gasteiger charges, as they are often used for proteins and other large biological molecules. During these preparatory steps, the mucin structure is improved and polished, giving a solid basis for effective molecular docking investigations. Then a simulation was performed using AutoDock Vina. All the nine suitable binding locations with their affinity were obtained from the simulation data. Finally, the LigPlus software was used to visualize the presence of hydrogen bonding between the protein (mucin) and the polymeric mucin.

2.13. Nanoformulation viscosity

A rheometer (Lamy Rheology RM 200 touch, France, spindle R1) was used to measure the viscosity of the generated formulations at a temperature of 25 ± 2 °C.[47] The formulations were not diluted to perform the measurements. To quantify the viscosity of the eye drops, the viscosity data were modeled using the Ostwald-de Waele equation, which is derived from Newton's law of viscosity and has generally been used to describe the behavior of typical non-Newtonian fluids.

$$\mu = K(T)\gamma^{n-1}$$

where K (equal to the viscosity at 1 s^{-1}) is the flow consistency index (Pas^n) and is a function of temperature and n is the dimensionless flow behavior index (the fluid is pseudoplastic when $n < 1$). To determine the coefficients (i.e., K and n) of the Ostwald-de Waele equation, a power-law formula was used to best-fit the viscosity data of the sample.

2.14. Drop size measurement

To determine the average drop volume, 3 mL of the nanoformulation was transferred into a plastic dropper. The formulation was released by gently squeezing the dropper at a 45° angle from the horizontal plane until the required number of drops were obtained. The released droplets were carefully collected and imaged at free falling state under uniform lighting on a flat, non-absorbent surface. Following proper scale, the diameter of each droplet ($n = 10$) was measured using the ImageJ software. Assuming spherical geometry, the mean droplet volume (μL) was calculated based on the measured diameters. This method mimics the practical administration angle of ophthalmic formulations and provides a reliable estimation of drop volume.[48]

2.15. Redispersibility

The redispersibility of the nanoformulation was evaluated qualitatively. The test consisted of manually shaking the glass vial after keeping it untouched and steady for 3 weeks to check for possible sedimentation. The vial was tilted to 180° keeping it upside down. The process was repeated until the sediment dispersed uniformly. Based on the effort required to convert the sediment to homogenous suspension, the formulations were evaluated. The lower number of inversions required to homogenize corresponds to a higher redispersibility percentage. One inversion was considered as 100% easy to be redispersed. Every extra flip decreased the percentage of redispersibility by 5%.[49,50]

2.16. Long-term stability

Since long-term stability directly affects the shelf life, therapeutic efficacy, and commercial viability of a liquid formulation, it is an essential quality to test. Long-term storage stability of the nanoformulation was evaluated by visual inspection during a storage period of one year at room temperature (25 ± 2 °C, $60\% \pm 5\%$ relative humidity). Instability was defined by visual signs of phase separation or color change. Visual inspections were conducted monthly.

2.17. *Ex vivo* histology study

The biocompatibility of the produced sample was assessed by conducting hematoxylin and eosin (H&E) staining on corneal tissues obtained from goat eyes. A pair of eyes was collected from the same goat. Then, 1 mL sample was instilled on one eye and allowed to remain for 15 min before rinsing the eye with sterile PBS, while the other eye was used as a control. The corneas were extracted using surgical procedures. The removed corneas were treated with fixation, dehydration, embedding, and then sliced into pieces that were 5 μm thick. The central corneal thickness was assessed by measuring the distance between the epithelial and endothelial surfaces from the optical microscopic images using ImageJ with the corresponding scale bar.

2.18. *In vivo* Draize test and corneal histology

The Draize test, also known as irritation test and histopathology tests of cornea were used to examine the *in vivo* ocular biocompatibility of NPs. This test continues to be the primary method accepted by the regulatory agencies worldwide.[51] The biocompatibility of the CIP-loaded mucin nanoformulation (Mu-XG-CIP NP) was determined by the irritation test. In this experiment, 50 μL of formulation was administered to one eye of the rabbit for 4 times a day for a period of 7 days, and the other eye was used as control. The irritation of the eyes was scored according to the Draize scale.[52,53] Ocular changes were graded for indications of lacrimation, irritation, redness (erythema), edema, and any other ocular reactions. The animals were euthanized after the final observation, and the corneas were removed and stained with H&E for histopathological evaluation. All procedures were performed in accordance with established protocols with the approval of the Animal Care and Use Committee (ACUC) of the Department of Biomedical Engineering at Bangladesh University of Engineering and Technology (BUET) (Approval number: 2024/BME/05).

2.19. *In vivo* anti-inflammatory study

To analyze the anti-inflammatory property of the sample Mu-Gly NP, adult male rabbit of 1 kg was taken as the test subject. The Animal Care and Use Committee (ACUC) of the Department of Biomedical Engineering at Bangladesh University of Engineering and Technology (BUET) approved all protocols, which were followed exactly. The ACUC clearance number for these protocols is 2023/BME/01. The albino rabbit was kept at the animal lab of the Department of Biomedical Engineering,

BUET. The rabbit was kept in a cage with 12 h of light and 12 h of darkness and the room temperature was maintained at 23 ± 1 °C. The rabbit was sensitized with 2.5 mL of bovine serum albumin (BSA) solution at a concentration of 5 mg mL^{-1} through intramuscular injections for 3 days with 1 day interval. Sensitization was done to activate the immune system of the rabbit, so that its body could start to produce antibodies. An inflammatory rabbit eye model was created by injecting 0.05 mL BSA in the sclera of the rabbit eye. The process of challenging the left eye was performed under general anesthesia induced *via* intramuscular injection of ketamine hydrochloride (35 mg kg^{-1}). The application of drug dosage was started after 24 h of challenging. The rabbit eyes were examined post-challenge using an Alcon LuxOR® Revalia™ ophthalmic microscope at 7.5× magnification. The right eye remained unchallenged and is considered as control. For 3 days, 4 dosages at an interval of 3 h have been given to the left eye. Then, 50 µL per dose was applied to the eye topically. The condition of the eye was observed visually and scored according to the severity. The iris inflammation was scored following the scale mentioned previously by a research group where scores 0, 1, 2, 3 and 4 correspond to no response, slight redness, mild redness, moderate redness with mild edema, and marked redness with moderate edema of the eye, respectively.[54]

2.20. *In vivo* bacterial infection model

Four male New Zealand white rabbits, aged approximately four months and weighing 1.2–1.6 kg, were purchased for the experiment. The animals remained in individual cages throughout the period of adaptation (1 week) and experimentation (7 days) at 25 °C, and the 12 h day/12 h night cycle was maintained. There was no restriction of water or food during the experiment. The animals were divided into three groups after infection with bacteria: positive control (received no treatment), treated (received ciprofloxacin-incorporated xanthan gum-based mucin nanoformulation) and control (received commercial eye drop from Aristopharma®). The study was approved by the Animal Care and Use Committee (ACUC) of the Department of Biomedical Engineering at Bangladesh University of Engineering and Technology (BUET) (Approval number: 2024/BME/03). The rabbits were anesthetized with intramuscular combination injection of ketamine hydrochloride (30 mg kg^{-1}), and the eyes were topically anesthetized with 0.5% procaine. To induce unilateral infection, 37×10^8 colony-forming units per mL (50 µL) suspensions of *Staphylococcus aureus* isolates in logarithmic growth phase were injected into the sclera of the eye. The injection was performed with a 30-gauge needle and retained for 30 s to ensure the uniform spearing of the bacteria (Day 0). Since *S. aureus* is a common source of bacterial infection of the cornea and ocular surface infections and is frequently employed in preclinical models to create reproducible corneal infections for assessing ophthalmic treatments, it was chosen as the infectious agent as per established methods.[55,56] Treatment was initiated on the day after bacteria inoculation (Day 1). Rabbits (n = 2) in a positive control group were injected with *S. aureus* to cause infection, yet they were not given any kind of treatment. For the treatment of infection model, ciprofloxacin

loaded (0.3% w/v) in Mu-XG NP was administered at a dose of 50 µL per eye, four times daily (08:00, 12:00, 16:00, and 20:00) for seven consecutive days. To evaluate the therapeutic efficacy of the two formulations, *i.e.*, mucin NP and commercial eye drop, corneal clouding was used to categorize the clinical signs of the severity of bacterial infection. It ranged from a clear cornea (0) to different levels of edema. The grade for minor edema was 1, and the grade for corneal edema that affected two quadrants or almost 50% of the total ocular surface was 2. Grade 3 was assigned to the most severe stage, which was complete corneal clouding. A double-blind trial was performed by two independent researchers to evaluate the pathological changes in the conjunctiva. Conjunctival redness, discharge and lid edema were assessed daily by two independent blinded investigators using a 0 - 4 scale according to a scale in which a 0 score indicates no signs; 1, slight signs; 2, mild signs; 3, moderate signs; and 4, severe signs.

2.21. Corneal histology

Immediately after sacrifice, one part of the cornea was removed and kept in 25% formaldehyde solution. Corneas embedded in paraffin were sliced into 4-µm-thick cross sections by using a microtome. These sections were placed on a slide and dried overnight in an oven at 60 °C. After removing the paraffin from the slides using xylene, the tissue was washed with water and alcohol. The samples were stained with nuclear dye for 10 min, rinsed and then counterstained with eosin. These slides were then washed in a reverse manner (running water, alcohol, and xylene), cover slipped, and examined under a light microscope (Olympus CX41). Eyes that received mucin NP formulation were compared with those from the positive control (no treatment) and commercial eye drop group.

2.22. Field emission scanning electron microscopic (FESEM) images of corneal surface

The removed corneas were also prepared for FESEM scanning. The samples were first fixed with 2.5% glutaraldehyde for 2 h keeping at 4 °C, followed by three washes by vortex in PBS for 15 min each. The samples were then dehydrated by a graded series of ethanol (30%, 50%, 70%, 80%, 90%, 95% and 100%) for 15–20 min each and subjected to FESEM examination. The surface of the cornea was assessed by FESEM examination (Sigma VP300).

2.23. *In vivo* pharmacokinetic study

The *in vivo* pharmacokinetic profile of the CIP-loaded mucin nanoformulation was investigated at a concentration of 0.3% (w/v) in the formulation applied in rabbit eye. The rabbits were administered with a single dosage (100 µL) of topical formulation into the lower conjunctival sac of the eye. At predetermined times, 150 µL of aqueous humor was collected using a 27G syringe, mixed with 500 µL of HPLC mobile phase containing water and acetonitrile at the 80:20 ratio, and the remaining protein in the sample was removed by centrifugation at 6000 rpm min^{-1} for 20 min. Finally, the CIP concentration in the aqueous humor was detected by the HPLC method using a UV detector at 280 nm.

3. Results and discussions

3.1. Mechanism of formation of mucin nanoparticles

Mucin nanoparticles are formed in a neutral pH medium dispersed in distilled water. In an aqueous dispersion of mucin, carboxyl groups of sialic acid (COOH) donate a hydrogen atom and become negatively charged. These groups attract the Ca^{2+} ions of $CaCl_2$ salt. Mucin is known to interact with calcium ions in many intracellular processes.[57,58] The same interaction occurs in the ionic gelation technique. Calcium-dependent cross-linkage forms between multiple mucin chains through sialic acid groups attached to the oligosaccharides, as shown in Fig. 1(i). Intramolecular disulfide bonds in the N-terminal region between two chains assemble the mucin chains. Due to this interaction between opposite charges, spherical mucin particles are formed.

3.2. Morphological analysis of mucin nanoparticles

ZP can be used to indicate the stability of formulated colloidal dispersions by determining the degree of repulsion force. A high repulsion force prevents particles from aggregation.[59] In addition, PDI indicates the extent of particle size distribution with a range of 0–1, and a PDI of less than 0.2 is often considered as narrow size distribution. Physiochemical parameters, such as particle size and zeta potential, are listed in Table 1. The morphological analysis for the prepared polymeric nanoparticles was performed by TEM, and the TEM images are displayed in Fig. 1(ii). The increase in mucin concentration affording more negatively charged functional groups can gather around the crosslinking agent named Ca^{2+}, and therefore, further layers of mucin chains can join the calcium cations, and thus, the size of nanoparticles increases with the increase in the mucin concentration.[60] The effect of crosslinker concentration on particle size is evaluated by varying Ca^{2+} concentration while keeping the

mucin concentration fixed at 1% w/v. With the increase in calcium ion concentration, lower numbers of the polymer chains are involved with higher contents of cations, and therefore, the size of nanoparticles decreased as expected. The cationic polymer, chitosan, was used as a crosslinker in place of the cationic salt $CaCl_2$, resulting in the formation of stable particles. Mucin nanoparticles crosslinked with different chitosan ratios showed a positively charged zeta potential. In the case of chitosan-crosslinked mucin NPs, the particle size ranged from 473 to 619 nm. The sizes of NPs are reported in Table 1. The particle size has increased with the amount of chitosan due to the large molecular weight of this amino polysaccharide.[61] The zeta potential of these nanoparticles is positive due to the exposure of free amino groups of chitosan chain.[62] The chitosan crosslinked with mucin nanoparticle samples having higher zeta potential and lower PDI values indicate a comparatively narrow particle size distribution and stable non agglomerated nano systems.[63] The deprotonated sialic acid groups present in the mucin chain contribute to its negative surface charge. The calcium-crosslinked mucin nanoparticle has very low ZP, and shows instability.

Negatively charged polysaccharides, i.e., xanthan gum (XG), gum acacia (GA) and gellan gum (GGL) have been mixed at 0.2% (w/v) and 0.5% (w/v) as stabilizers to achieve stable mucin nanoparticles. These polysaccharides and the mucin protein chain interact with each other to form a hydrocolloid and impart stickiness to the nanocarrier.[64] Only in the case of 0.5% XG, a moderately high zeta potential is attained. The purpose of improving the stability of the nanoparticles was achieved by adding XG. The mucin nanoparticles would otherwise exhibit instability over time, but it enhanced their shelf life, reduced aggregation, and raised their zeta potential. The adhesion of XG fragments to the particle surface is visible in the TEM image (Fig. 1). The particle size decreases after mixing XG and becomes less than 200 nm, which is highly desirable for enhanced penetration through the cell membrane. The other two gums yielded larger particles, and the values are given in Table 2. The more hydrophilic nature of GA than XG and GGL due to the presence of a large number of hydroxyl (–OH) functional groups attracts more water molecules in the three-dimensional network, consequently increasing the particle size of Mu-GA NPs.

The physical appearance and stability of the nanoformulation stored at 4 °C were further monitored over a period of two months, and no irreversible agglomerates were observed.

3.3. Pure and drug-loaded nanoparticles with drug entrapment efficiency and drug loading capacity

The antibiotic drug entrapped in the core of particles is clearly visible in the TEM images displayed in Fig. 1(ii). Ciprofloxacin

Table 1 Change in the zeta potential and particle size with respect to different concentrations and crosslinkers

Sample	Zeta potential (mV)	Size (nm)
10%Glycerol + 1% Mu + 1% Ca^{2+}	−1.84	868
1% Mu + 0.5% Ca^{2+}	−4.45	959
1% Mu + 1% Ca^{2+}	−4.39	797
1% Mu + 2% Ca^{2+}	−4.93	735
0.5% Mu + 1% Ca^{2+}	−3.05	507
0.25% Mu + 1% Ca^{2+}	−3.63	187
1% Mu + 1% CS (1:2)	+27.2	473
1% Mu + 1% CS (1:3)	+24.7	498
1% Mu + 1% CS (1:5)	+27.8	567
1% Mu + 1% CS (1:7)	+27	619

Table 2 Variation in the size and surface charge of mucin NPs for different gums

Concentration of gum	Xanthan gum		Gum acacia		Gellan gum	
	Particle size (nm)	Zeta potential (mV)	Particle size (nm)	Zeta potential (mV)	Particle size (nm)	Zeta potential (mV)
0.2%	181	−6	435	1	459	−15
0.5%	158	−27	670	−4	297	−2

remains in the core owing to its interaction with calcium ions.[65,66] Here calcium acts as a chelating agent ensuring maximum drug entrapment. Drug encapsulation is a technique to protect chemicals from degradation, control release, and target medicinal formulations. CIP-loaded mucin nanoparticles showed an entrapment efficiency of 95.51% ± 0.62%. This high DEE is due to the hydrophobicity of ciprofloxacin preventing its diffusion back into the aqueous medium from the core of Mu NPs. Mu NPs have a higher drug encapsulation efficiency than the other NPs reported in the literature because of the incorporation of drugs along with a cationic crosslinker.[67,68] In this case, the drug is mixed with the crosslinker solution as stated in the earlier section, and hence, drug particles remain near the calcium molecule and at the end of electrostatic interaction, the drug becomes entrapped in the core of the nanoparticle. The drug loading capacity of dried nanoparticles was 12% ± 6.4%.

3.4. Redispersibility index and drop size

The redispersibility of Mu NPs was assessed as part of their stability evaluation. The test was conducted three weeks post-formulation to evaluate the tendency of particulate matter to settle at the bottom of the glass vial and the ease with which the settled particles could be redispersed into the solution. For the Mu-XG nanoformulation, no sedimentation was observed even after three weeks of storage, indicating 100% redispersibility. The solution remained homogeneous upon inversion of the vial as shown in Fig. 2a, indicating excellent stability and resistance to particle aggregation. This suggests that the synthesized nanoformulation has achieved strong steric or electrostatic stabilization, preventing phase separation, and the result can be correlated with the obtained zeta potential (−27 mV) value. For the Mu-Gly nanoformulation, visible sedimentation was observed at the bottom of the vial upon inversion, suggesting weaker stability in the suspension over the storage period. To redisperse the sedimented particles, the vial required two inversions having 80% redispersibility score. After these rotations, the solid particles appeared to mix uniformly into the solution, restoring homogeneity. This behavior indicates that while sedimentation occurred, the particles retained redispersibility but did not form irreversible aggregates. The difference in sedimentation behavior between the Mu-XG and Mu-Gly formulations is due to their distinct physicochemical properties such as particle size, zeta potential, and the interaction between the polymer matrix and the mucin nanoparticles. The absence of sedimentation in Mu-XG suggests high colloidal stability. From Fig. 2b, the diameter of free falling droplet was measured, and hence, the volume was calculated. The drop size of Mu-Gly NP and Mu-XG NP is 54 ± 16 μL and 84 ± 30 μL, respectively. The higher volume of Mu-XG NPs is due to the strong cohesion force and highly viscous nature, enhancing the surface tension.

3.5. Viscosity

While prolonged residence times are achieved by increasing the viscosity, there are a number of shortcomings, including discomfort and blurring. To prevent the lubricants from being removed from the ocular surface, the ideal formulation should theoretically be viscous at low shear rates, such as when the eyes are opened. To reduce friction, irritation, and ocular discharge, the viscosity should be low during high-shear situations like blinking. Consequently, non-Newtonian artificial tears that exhibit shear-thinning behavior, which is viscosity that decreases with the increase in shear rates, are preferred.[69] Low-viscosity eye drops at low shear rates are more likely to evaporate quickly and to drain rapidly. However, a lower viscosity of the eye drops is needed at higher shear rates, including when blinking, to enhance wearer comfort and lessen inflammation caused by friction.[70] One approach is to use high-molecular-weight polymers to increase the viscosity of the formulations, which will increase the residence time and bioavailability of artificial tears.[71] Only Mu-XG nanoformulation shows shear thinning behavior due to the presence of XG in it. The reason for the formation of extremely shear-thinning solutions with XG is either the intermolecular connections of two or more molecules, or the stiffness of its molecules. The stretched polysaccharide molecules intertwine to create clumps that result in high viscosity at low shear rates. As the shear rate increases, the aggregates disintegrate, the molecules align with the flow direction, and the apparent viscosity decreases.[72,73] From rheological analysis, XG represents shear thinning also known as pseudoplastic behavior, with viscosity decreasing with the increase in shear rate. In contrast, the pure Mu, Mu-Gly, and Mu-GG dispersions displayed Newtonian to slightly shear-thinning behavior, maintaining a nearly constant viscosity across the tested shear rates, given in Fig. 2d. The shear thinning behavior of Mu-XG is compared to the equation of power law model, and it is found that the correlation factor is 85%, the coefficient K is 784.55 Pa-s and the value of dimensionless n is 0.69, confirming the pseudoplastic behavior.

3.6. ATR-FTIR

Fig. 2f shows the ATR-FTIR spectra of empty Mu NP, drug-loaded Mu-XG NP and drug-loaded Mu NP. The analysis of the ATR-FTIR spectrum revealed broad peaks ranging from 3250 to 3280 cm^{-1}, which indicate the presence of O–H groups. The ATR-FTIR spectrum of mucin nanoparticles shows that principal peaks at wave numbers of 1076.1, 1238.6, 1640.8, 2928.2, and 3272.3 cm^{-1} correspond to C–N vibrations, –C–O stretching, N–H bending, C–H stretching, O–H stretching, respectively. The drug-incorporated NP sample has a peak at a wavenumber of 2850 cm^{-1} corresponding to aromatic cyclic enes. The new peaks in the region of 2900 cm^{-1}, 1720 cm^{-1} and 1400 – 1500 cm^{-1} confirm the presence of drug ciprofloxacin in the Mu-CIP sample. The peak in the Mu-XG-CIP sample in the 1623 cm^{-1} region has a higher intensity representing the C=O stretching in the 4-quinolone ring of the present ciprofloxacin molecule. However, no chemical interaction between the drug and the mucin polymer is evident.

3.7. Drug release study

The decrease in the rate of deterioration allows reducing medicine doses, which can reduce potential side effects. Controlling
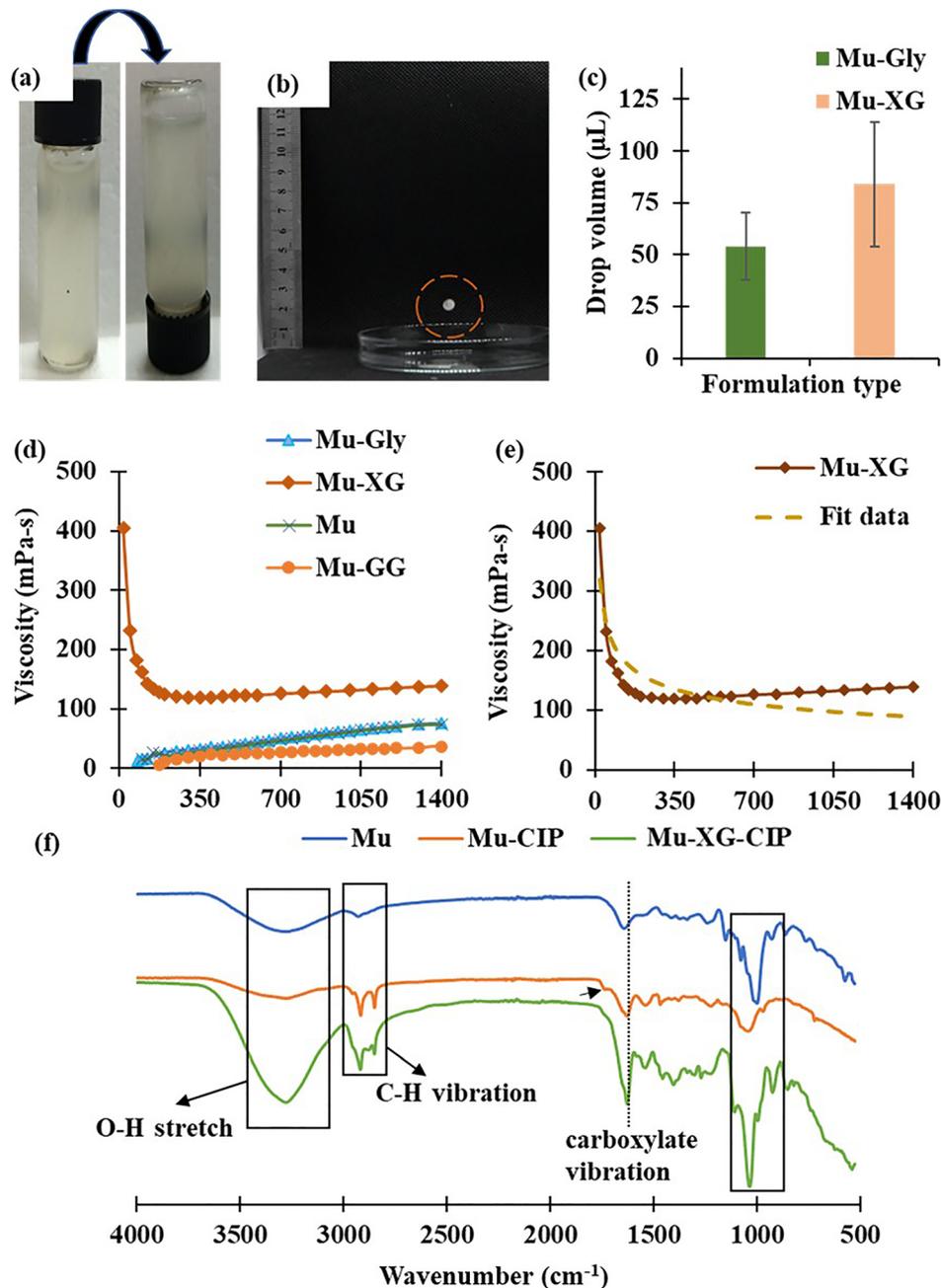
Fig. 2 Physicochemical properties of the developed mucin nanoformulation. (a) Inversion technique to check for redispersion, (b) a free falling droplet of mucin nanoformulation, and (c) volume of a drop of Mu-XG NP much higher than Mu-Gly NP. (d) Effect of xanthan gum on the viscosity of the formulations, making it shear thinning, whereas pure Mu NP, Mu-GG, and Mu-Gly nanoformulations show a shear thickening behaviour. (e) Mu-XG follows the pattern of power law model of viscosity with 85% correlation. (f) ATR-FTIR spectra of Mu, Mu-CIP and Mu-XG-CIP showing successful incorporation of CIP.

the release of drugs is an appropriate option for prolonged treatment. It reduces the number of administrations and maintains a steady plasma concentration profile for a long time. The Mu-XG nanoformulation shows lesser release over time compared to the other formulations, as shown in Fig. 3a. Natural excipients such as glycerol act as an osmotic agent in the formulation and increase drug release.[74] XG forms a hydrophilic

matrix, the drug release rate from matrices decreases due to the increase in the viscosity and thickness of the hydrated gel layer and around 15% drug is released over the 30 h study period. This gel barrier restricted water penetration into and drug diffusion from the particle, delaying drug release to achieve sustained release.[35,75,76] The higher viscosity of XG forms a diffusion barrier, slowing drug molecules' passage from the matrix to the
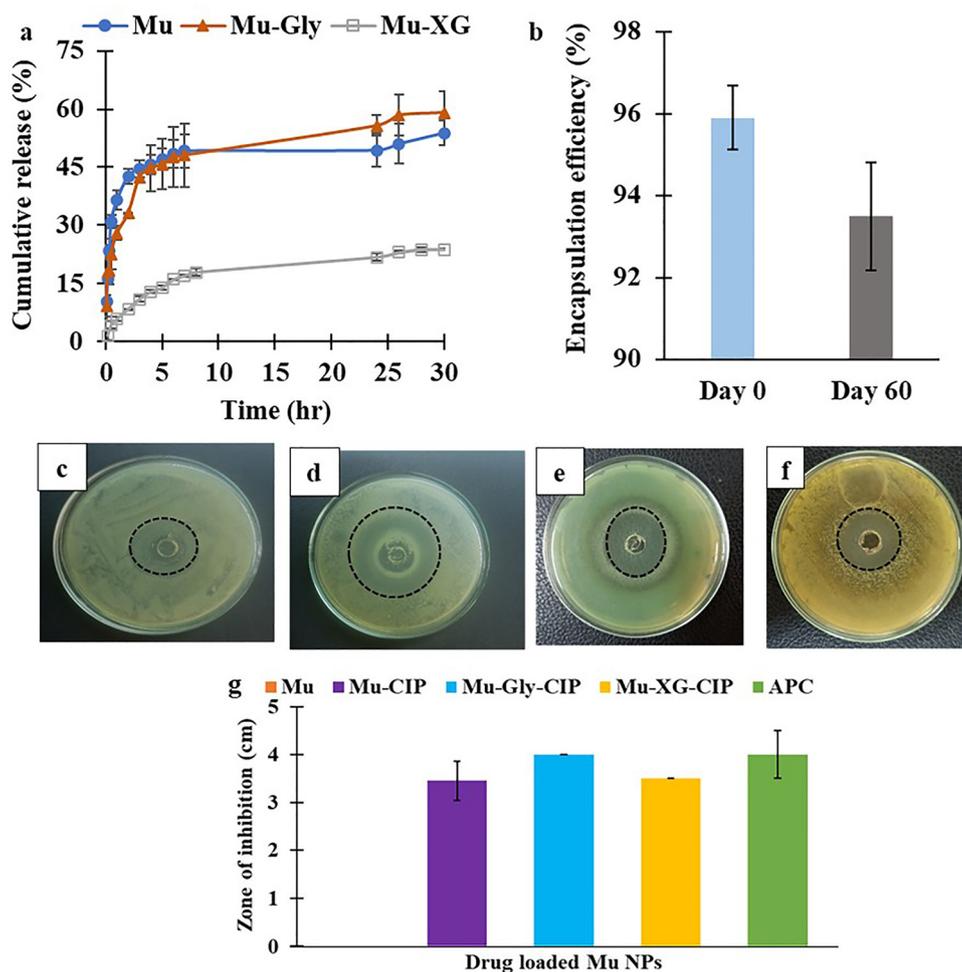
Fig. 3 Properties of the mucin nanoparticle as an effective drug carrier. (a) *In vitro* release profile of ciprofloxacin from the pure Mu NP, Mu-Gly NP and Mu-XG NP in PBS. Cumulative amounts of ciprofloxacin (%) are released from nanoformulations (mean $\pm$ SEM; n = 3). Mu-XG nanoformulation succeeded in slowing and sustaining the release of drug; however, the other formulations exhibited a higher release of 50% of the drug in the first few hours. (b) Extended drug encapsulation ability in the core of NPs over time with no significant difference compared to the freshly prepared sample. It represents a good sign of longer shelf life. Antibacterial activity of nano formulations against *S. aureus*. Zone of inhibitions of (c) Mu-CIP, (d) Mu-Gly-CIP, (e) Mu-XG-CIP, and (f) APC. (g) Bar plot representation of the diameter of zones of inhibition for different formulations, where the mucin formulations are equally successful as the commercial eyedrop.

surrounding medium. When xanthan gum hydrates the surface, it produces a highly viscous coating around the NPs. This layer regulates the penetration of the solution and limits drug diffusion, lowering the rate of drug release. Moreover, the entanglement of XG chain works as an obstacle to drug release. The surface area of a particle is directly dependent on its size, which is correlated with the drug release rate.[77] The small particle size increases the formulation's surface area and increases the drug release rate. Larger particles are ideal for prolonged and sustained drug release since they encapsulate more of the drug due to their massive core.[78] From the drug release profile given in Fig. 3a, it is observed that almost 50% drug is released within the first 7 h from Mu NPs after which a plateau is obtained. Thus, this profile shows controlled release of drug from the polymer matrix. Anion exchange between CIP and phosphate anions in the release media is the process that occurs during drug release.[79] Drug release *via* degradation can also occur from within the bulk

polymeric system when both the hydrophobic and hydrophilic regions in the polymer backbone are present.[80] Drug release profiles can generally be divided into two segments: an extended diffusion-controlled phase and an early burst. The drug is released from the polymer matrix due to the interaction between the NP and PBS, where the initial gradient of drug concentration is high, which provides a strong driving force for diffusion. The CIP-loaded mucin NP shows drug release by diffusion at first and then bulk erosion of the polymer chain, as suggested by the increase in the turbidity of the release medium after 24 h.

The release mechanism for the CIP from the Mu-Gly-CIP NP and Mu-XG-CIP was estimated using five models to fit the experimental cumulative drug release data. The kinetic parameters are listed in Table 3. At pH 7.4, the best-fitting model was the Korsmeyer–Peppas model, which had the highest R^2 values. The Mu-XG-CIP formulation has more similarity to the Korsmeyer–Peppas model due to the higher correlation factor

Table 3 Kinetic model parameters for ciprofloxacin release from two types of nanoformulations

| Drug CIP | Zero order R^2 | First order R^2 | Higuchi R^2 | Korsmeyer–Peppas | | Hixson R^2 |
				n	R^2	
Mu-Gly-CIP	0.60148	0.60157	0.76277	0.162	0.8994	0.60148
Mu-XG-CIP	0.8832	0.8832	0.9601	0.351	0.9800	0.88322

(98%) than that of the Mu-Gly-CIP formulation. The Korsmeyer–Peppas model is also known as the power law model, which is a semi-empirical model based on the diffusion phenomenon.[81] This model is developed to describe the drug release mechanism from polymeric systems. The release exponent n indicates the type of diffusion of the release mechanism. For Fickian diffusion, n is less than 0.5, implying that drug release by the diffusion-controlled penetration of solvent into the polymer-crosslinker matrix is much faster than polymer chain relaxation.[82] However, $0.5 \leq n \leq 0.89$ denotes non-Fickian transport, $n = 0.89$ denotes Case II (relaxational) transport, and $n > 0.89$ denotes Super Case II transport.[37] A low value of n presented in Table 3 supports the Fickian diffusion of ciprofloxacin from mucin nanoparticles.

Mu NPs serve as the excellent drug carrier due to its extended shelf-life. The drug encapsulation efficiency of Mu NPs does not significantly degrade over time even after 2 months, as depicted in Fig. 3b.

3.8. Antibacterial property testing

The effectiveness of the nanoparticle as an antibiotic system was evaluated against *S. aureus* using the well diffusion test. No inhibition zone for pure Mu NPs without drug is visible on the agar plates, showing that the components of the mucin polymer chain do not possess antibacterial activity. The test results of three different formulations of mucin with the same concentration of antibiotic are given in Fig. 3c to f. Drug-loaded Mu-CIP NPs exhibit an inhibitory zone of 3.46 ± 0.41 cm. The hydrophilic gel system of the agar plate has a stronger affinity for hydrophilic substances like glycerol, which enables diffusion through the gel network to quickly kill bacteria.[83] This offers compelling evidence of an increased inhibitory zone of 4 ± 0 cm for Mu-Gly-CIP NPs. The slower drug release from Mu-XG-CIP NPs results in a decrease in the zone diameter, which is 3.5 ± 0 cm. The commercial eye drop Aprocin (APC) from Aristopharma® shows 4 ± 0.5 cm zone of inhibition. The nanoformulation Mu-XG-CIP NP exhibits similar performance compared to the commercial product (p-value > 0.05, ns), as shown in Fig. 3g.

3.9. *Ex vivo* mucoadhesion test analysis

Mucoadhesion is done on excised goat eyes for three incremental concentrations of mucin (*i.e.*, 0.5%, 1% and 1.5%), and the other two formulations are 1% mucin mixed with 0.5% xanthan gum-coated Mu-XG and commercial eyedrop Aprocin®. Increasing the mucin concentration from 0.5% to 1% improves mucoadhesion as a higher concentration of polymer makes the formulation denser and more viscous, as given in

Fig. 4a. Further increment from 1% to 1.5% results in reduced mucoadhesion. In all three instances, the same trend is seen. The reason behind is the repulsion force between negatively charged epithelia and highly concentrated negatively charged mucin polymers. The Mu-XG formulation shows high surface tension and the droplets tend to stick to each other due to cohesive force. As a result, the repeated trials show a lower standard deviation. Mucin nanoformulation has a higher mucoadhesivity than that of the commercial formulation. The mucoadhesion of Mu-XG is significantly higher ($p < 0.05$) than the market eye drop, as depicted in Fig. 4b. The topical application of mucin nanoformulation interacts with the glycoprotein present on the ocular surface, allowing the spreading of sample over the surface and then the penetration occurs through diffusion. Diffusion increases with the surface area. Every mucin polypeptide chain has domains rich in serine and/or threonine, with hydroxyl groups linked to oligosaccharides through an O–glycosidic bond, and the glycosylated domains are devoid of secondary structures.[84] As the core protein of mucin is made up of tandem sequences that are abundant in O–glycosylated serine and threonine as well as proline residues, their long structures make the chain less flexible than unglycosylated random coils. These characteristics explain the rigid structure of mucin, high buoyant density, high hydrodynamic volume, and high viscosity.[85] The results from molecular docking support the cause of high mucoadhesion of mucin NPs. The results of molecular docking and the LigPlus software confirm the H-bond interaction between ocular mucin and the present mucin polymer in the NP. In Fig. 4c, the dotted lines represent the newly formed hydrogen bond. These interactions provide a molecular basis for the enhanced mucoadhesion observed experimentally. Fig. 4d shows the simulation results on the optimum position of molecular docking with the highest affinity. The position with the highest affinity has the lowest binding energy (-6.1 kcal mol^{-1}), giving the most stable position.

3.10. Long-term stability analysis

Visual inspection confirmed the excellent stability of Mu-XG NPs. However, pure Mu nanoformulation showed phase separation after a month, although the two phases could be remixed by shaking. The Mu-XG formulation is stable at both 4 °C and 25 °C, as no signs of instability (particle aggregation, creaming) were seen, whereas it exhibited color change at 40 °C. The images are given in the SI Section (Fig. S1).

3.11. *In vitro* hemolysis ratio analysis

The findings of the hemolysis test, which are depicted in Fig. 5(i), indicated that there was almost no hemolysis reaction. Both Mu-Gly NP, Mu and Mu-XG NP hemolyze at rates of $1.46\% \pm 0.71\%$, $1.7\% \pm 0.83\%$ and $3\% \pm 0.83\%$, respectively. The statistics show that these nanoparticles have excellent biocompatibility since they fully satisfy the requirements of the international standard for biomaterial hemolysis rate of less than 5%.[86] Triton X-100 (positive control) caused the extreme damage and lyses of every RBC and PBS (negative control), which showed the precipitation of healthy and intact
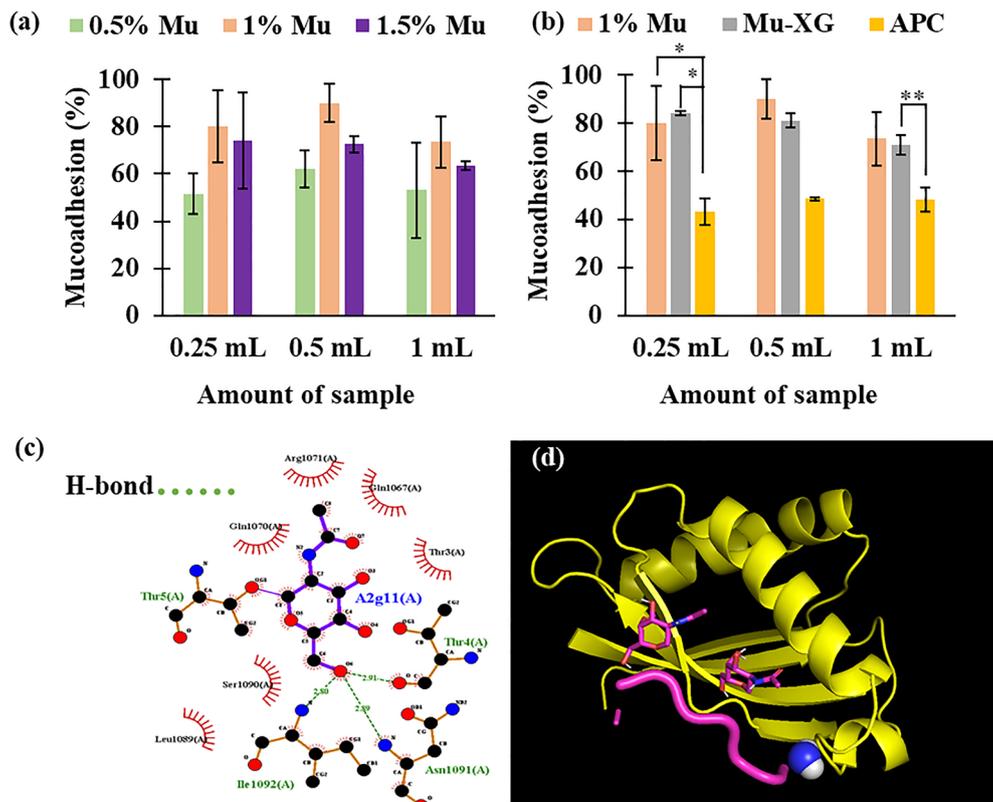
Fig. 4 Mucoadhesiveness of the mucin nanoformulation. (a) Comparative *ex vivo* mucoadhesion levels at different amounts of applied sample. With the increase in the concentration of mucin, there is an increase in mucoadhesion to a certain level and then it decreases. (b) Mu NP and Mu–XG NP have significantly higher mucoadhesion than the commercial equivalent APC. (c) Molecular docking analysis between ocular mucin and polymeric mucin confirms the presence of hydrogen bonding (green dotted lines). (d) Representation of binding between these proteins at the best possible site.

RBC at the bottom of the tube. Mu NP, Mu-Gly NP and Mu-XG NP formulations were similar to the negative control proving their biocompatibility. Nanoparticles consisting of chitosan and mucin exhibited a high hemolytic ratio due to the use of the acidic medium for chitosan dissolution. The neutralization of the medium after the formation of nanoparticles adds a complexity in procedure, and hence, these chitosan-mucin nanoparticles are excluded from other *in vitro* studies despite having high stability.

3.12. *In vivo* Draize test and corneal histology

The Draize test revealed that there were no abnormalities in the cornea, iris, or conjunctiva of rabbit eyes as a result of administering multiple doses of Mu-XG-CIP NPs. Additionally, there were no noticeable differences in the corneal regions of the eyeballs treated with mucin NPs compared to the control eye (Fig. 5(ii)), indicating that the formulation is entirely biocompatible and non-irritating. The same rabbit's cornea is assessed for further evaluation of biocompatibility. The cornea is composed of five layers,[87] namely, the corneal stratified squamous epithelium (i), Bowman's membrane (ii), stroma consisting of collagen fibers and keratocytes (iii), Descemet's membrane (iv), and the endothelium (v). The corneal epithelium and stroma of the rabbit treated with Mu NPs for one week were completely intact, as observed from the H&E staining, and remained attached to

Bowman's membrane, without any signs of edema, as shown in Fig. 5c.

3.13. *Ex vivo* histology analysis

The histology of goat corneal tissue shows that corneal layers (epithelium, Bowman's membrane, and stroma) remained intact with and without drug-loaded mucin NP sample. No desquamation of corneal epithelium is observed, but a slightly edematous stroma is observed in the H&E assay. Fig. 5 a and b represent the histology images of goat cornea after applying the Mu NP and Mu-CIP NP formulation. The morphology of the cornea is determined to be in good shape, and there is no loss of tissue integrity even after applying the sample. Corneal epithelial cells take up the particles by endocytosis. No toxicological features were observed in the cornea including the epithelium and the stroma even after keeping the formulation for 30 min as compared with normal DI water. The histopathological findings support the use of mucin nanoparticles for ophthalmic application. The total thickness of the central cornea and epithelial layer is measured, and the ratio of epithelium to total corneal thickness is calculated as well. The ratio was measured to be 0.15, and thus, there was no significant increase in thickness upon applying the drug-loaded nanoformulation to the excised eye compared to the control, suggesting that the nanoformulation did not cause any damage.
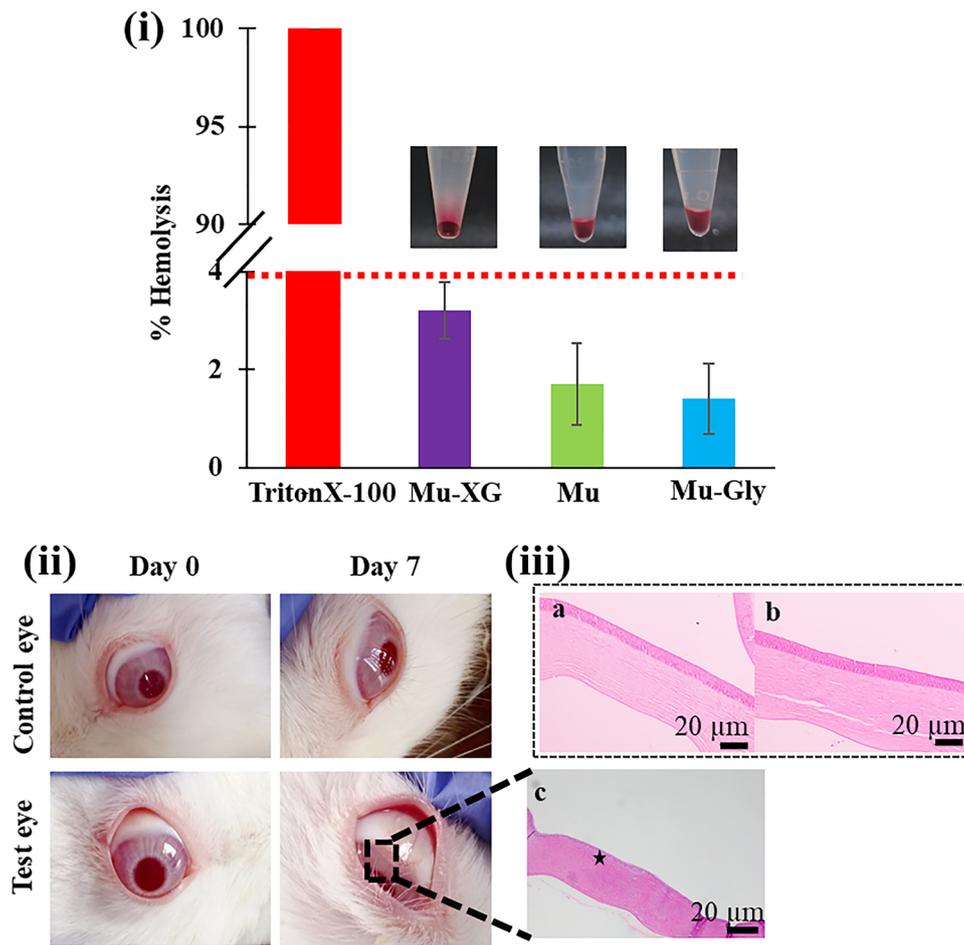
Fig. 5 Biocompatibility analysis of mucin nanoparticles. (i) Hemolysis ratio of Mu, Mu-Gly and Mu-XG nanoformulations and positive control (Triton X-100) with the images of supernatants of intact healthy RBCs. (ii) No signs of possible visual irritation are observed in rabbit eyes after applying the developed nanoformulations for seven consecutive days. (iii) H&E histological staining of excised goat cornea after applying the pure mucin nanoformulation (a) and ciprofloxacin-loaded nanoformulation (b) shows intact epithelial layer and stroma. In the rabbit corneal histology of the test eye on day 7 (c), the asterisk (*) symbol highlights the intact epithelial layer with no swelling in the stroma layer.

3.14. *In vivo* anti-inflammatory property study

Inflammation was visible in the sclera of the challenged left eye of the rabbit after 24 h. After the successful inflammation induction, the eye condition was observed each time after the NP formulation administration. The right eye was kept untouched throughout the experiment. The rabbit was healthy and had no trouble opening its eyelid. After day 1, there was no noticeable alteration in the challenged eye and the condition of the right eye (negative control) was completely normal. There has been an obvious improvement since day 2. The inflamed zone was smaller than that on the first day of sample administration, and the redness begun to fade. On day 3, there was further progress, and the rabbit fully recovered. No increase in body temperature or discomfort in the rabbit eye was noticed throughout the entire procedure. Fig. 6(a) shows the healthy eye, Fig. 6(b) shows the image taken right before starting the treatment and Fig. 6(d) shows the image taken at the end of treatment, in which there is no red inflamed area. Fig. 6(e) shows the gradual decrease in inflammation during 3 days of treatment. The presence of glycerol and mucin in the solution,

which has a soothing impact in cases of discomfort, is the driving force behind healing. Type II mucin is a gel-forming mucin that plays a protective role in inflammation. Further addition of glycerol helps in lowering corneal edema and haze and facilitates better healing of the epithelium, endothelium, and their basement membranes, or corneal lamellae. It may not have been able to return to normal without treatment in case of inflammation because of fluid pressure in the intercellular or interlamellar spaces. Therefore, regular use of pure glycerol drops may restore relative deturgescence and corneal clarity in some cases of chronic corneal edema. The application of glycerol present in the formulation has increased hydration and inhibited lymphocyte accumulation close to the treatment site, which helped in healing.[88]

3.15. *In vivo* bacterial infection healing ability

The *in vivo* antibacterial efficacy of the developed nanoformulation was evaluated in a rabbit model of infection by *S. aureus.* Inflammatory mediators released at the site of infection rapidly diffuse into the aqueous humor, directly impacting other regions,
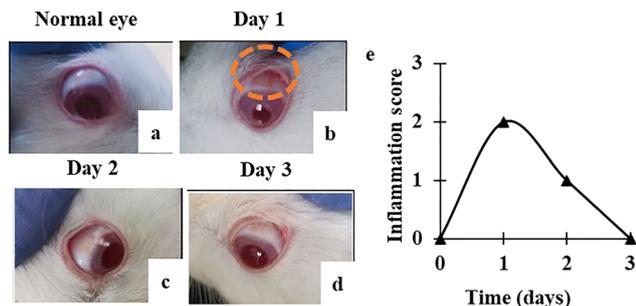
Fig. 6 *In vivo* therapeutic efficacy of Mu-Gly-CIP NPs against inflammation. Digital images of the rabbit eye at different time intervals under treatment: (a) healthy eye, (b) 24 h post-challenge and before the start of treatment, and (c, d) progression of healing of inflamed area where redness is diminishing gradually. (e) Qualitative inflammation scores up to day 3.

causing progression of ocular infection.[89] The rabbits from the positive control group kept their eyes closed with constant mucoid discharge, and the animals were euthanized on day 4 due to severe infection. Inflammatory cells, mostly neutrophils (shown by green triangles in Fig. S2), had widely infiltrated in corneal tissue. The therapeutic capability of the developed nanoformulation was assessed against a commercial eyedrop in rabbit models of bacterial conjunctivitis. The inoculation of *S. aureus* into the sclera in rabbits' eyes created severe clinical signs mainly in the cornea, conjunctiva, and iris. Peak infection was observed 24 h post-inoculation, and there was problem in opening the eyelid. The eyelids were swollen and the conjunctiva was red on the 1st day. On the following day, there was no noticeable change in redness, but there was a slight improvement in opening the eyelid and the sample application was ongoing. The 3rd day showed a similar trend to that observed on the previous day. On day 4, the rabbits could keep their eyelids open without difficulty and there was less purulence in the morning. On the 5th day, less redness was observed in the conjunctiva, and the rabbits always kept their eyes open comfortably. Finally, on the 7th day, the redness of the conjunctiva was almost completely resolved, and the conjunctiva had returned to its normal whitish color, as shown in Fig. 7(i). The rabbits treated with commercially available eyedrops had shown a similar pace in the improvement of bacterial infection. These visual observations suggest that the 0.3% CIP-loaded mucin nanoformulation has the same therapeutic efficacy as that of the market product. A clinical scoring index summarizing these observations is depicted in Fig. 7(ii) for a comparative analysis.

3.16. Corneal FESEM

FESEM observations reveal clinical improvement and elimination of bacterial cells. From Fig. 7(iii (a)), the intact cell junctions of hexagonal squamous cells of the upper corneal layer confirm the biocompatibility of the nanoformulation. Infecting bacteria can be identified using a SEM.[90] The deformed shape shows effective bacterial death caused by the Mu-XG-CIP nanoformulation; otherwise, live bacterial cells would be clearly visible on the cornea in Fig. 7(iii (b)).

3.17. Corneal histology analysis

At the end of the experiment, corneas were collected after rabbit euthanasia and sent for histopathological evaluation. The histological study showed normal cellularity in all corneal layers without signs of inflammation in both nanoformulation-treated eyes and negative control eyes, whereas the presence of inflammatory cells was observed in the commercial eyedrop (APC) treated eye in Fig. 8(a). The thickness of the total epithelial layer is also significantly higher due to swelling ($p < 0.001$), as shown in the bar plot of Fig. 8b. Bacterial infections often cause inflammation. From a time-course analysis in a study, it is found that inflammation peaked at 24 h after infection and decreased significantly at 48 and 72 h. Additionally, inflammatory cytokines were significantly reduced at these times.[91] The histology result illustrates that a commercial eye drop would require two to three extra days to eradicate all the inflammatory cytokines and neutrophils and complete the healing process eventually. It is observed that therapeutically, the Mu-XG NP exhibits superior efficacy in treating bacterial uveitis by mitigating the ocular inflammatory reaction.

3.18. *In vivo* pharmacokinetic analysis

Fig. 8c depicts the pharmacokinetic profile, which is the ciprofloxacin concentration in the rabbit aqueous humor at various time frames after instillation of 100 μL nanoformulation. The aqueous humor drug concentration increased slowly as expected according to the *in vitro* drug release highlighting the sustained release nature. From 2 to 6 h of initial administration, the drug concentration ranged from 0.24 to 1.14 μg mL^{-1}. The diffusion of ciprofloxacin from the mucin nanoparticles' inner core becomes noticeable after the liquid particle matrix allows deeper entrapped drug to spread outward, which is responsible for the significant rise in drug concentration after 4 h. This delayed release is consistent with the diffusion-controlled release behavior typically reported for polymeric nanoparticle systems. Even after 8 h, a significant amount of drug (0.26 μg mL^{-1}) is present in the aqueous humor for effective protection against bacterial growth reducing the necessity of frequent administration, as shown in Fig. 8c. The clearance of drug particles from the aqueous humor is shown by the drop in eight hours. However, in the case of the commercial ciprofloxacin eye drop, the drug concentration in the aqueous humor becomes 8 ng mL^{-1}, suggesting reapplication every 6 hours for better healing. After 8 h, the remaining free drug was below the detectable limit when administered without a carrier. Nanocarrier-based drug delivery enhances the transport of drug molecules through the cornea over time, as it adheres to the surface tightly without getting washed out.

4. Conclusion

A novel approach to preparing mucin nanoparticles in the ionic gelation procedure has been investigated in this study. Besides the information regarding morphological properties for various concentrations and different crosslinkers, this study provides a
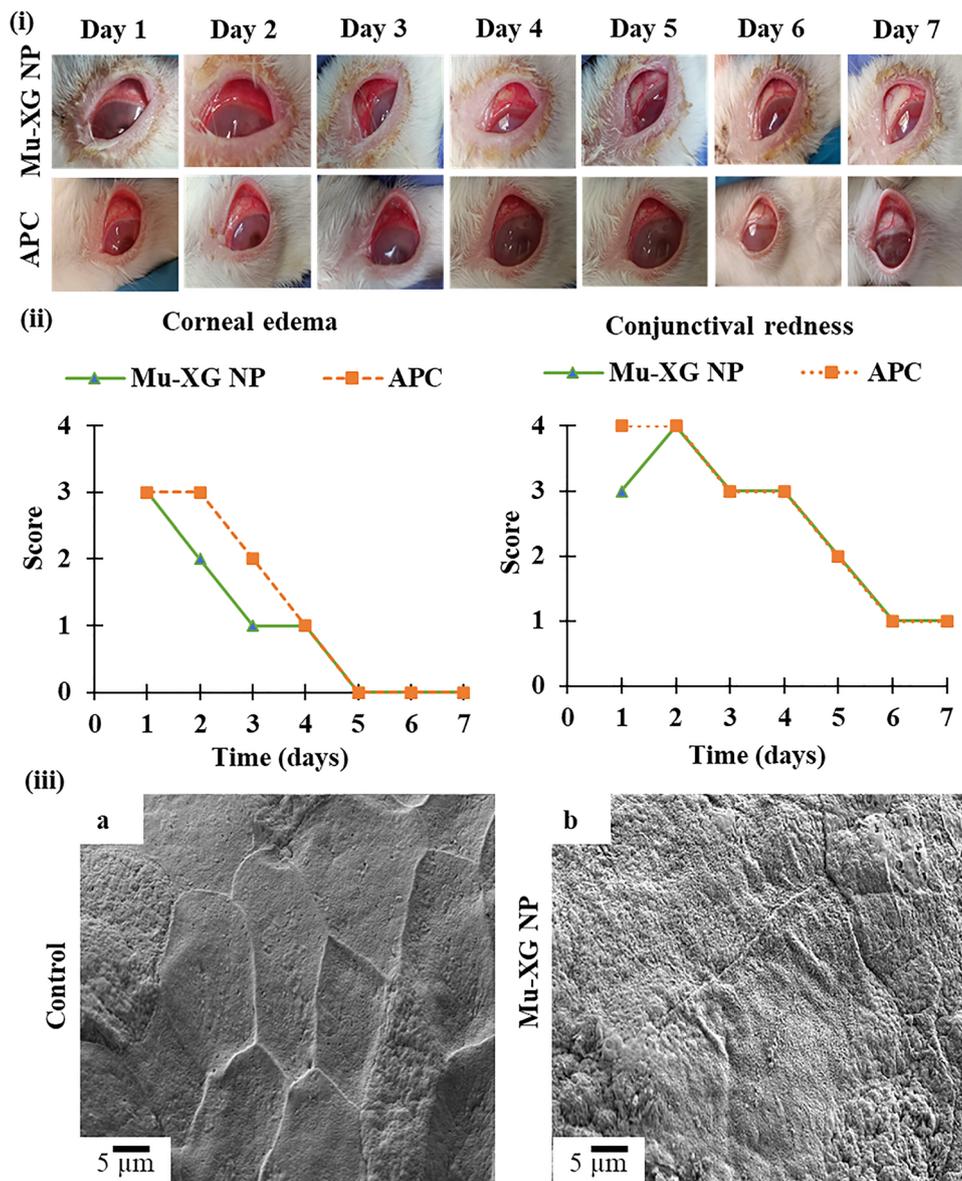
Fig. 7 *In vivo* performance of the CIP-loaded Mu-XG NP in healing bacterial infection. (i) Digital images of the rabbit eye under treatment with ciprofloxacin-loaded mucin nanoparticles and the commercial eyedrop Aprocin at different time intervals. (ii) Treatment results in the visual scoring of eyelid edema and redness during the healing phase, where the nanoformulation follows the same trend as the commercially available ciprofloxacin eye drop ($n = 2$, biologically independent eyes for each group). No significant difference in the healing efficacy is found. (iii) FESEM images of the surface of corneas: (a) ideal surface of another healthy rabbit cornea, where intact hexagonal epithelial cells and cell junctions are signs of biocompatibility upon applying nanoformulation, and (b) treatment with nanoformulation has killed all the bacterial cells and their debris are attached to the surface.

foundation for further research on mucin nanoparticles incorporating drugs in controlled drug delivery applications in ocular therapy. Among all the synthesized formulations, the mucin nanoparticles (NPs) with acceptable biocompatibility based on hemolysis assay exhibited a negative zeta potential and were perfectly nanosized. The precorneal residence period is extended in part by the small particle size and negative zeta potential. The *in vitro* drug release study demonstrated controlled release for 24 h. The Mu NP has an encapsulation efficiency and a drug loading capacity of 95% and 12%, respectively. The mucin matrix offers intrinsic mucoadhesive interactions

and a hydrophilic milieu that promote greater drug entrapment, in contrast to other polymeric nanoparticles. The benefits of our method in terms of drug loading capacity and possible ophthalmic performance can therefore be more clearly assessed by benchmarking against acceptable carriers. The *ex vivo* corneal mucoadhesion of the NPs was proved to be promising without having a noticeable harmful impact on the corneal surface. The biocompatibility of the formulation was further confirmed by *in vitro* hemolysis assay, *ex vivo* histology of caprine cornea and the *in vivo* Draize test. An *in vivo* inflammation model of rabbit eye was developed, and after applying drug-loaded nanoparticles,
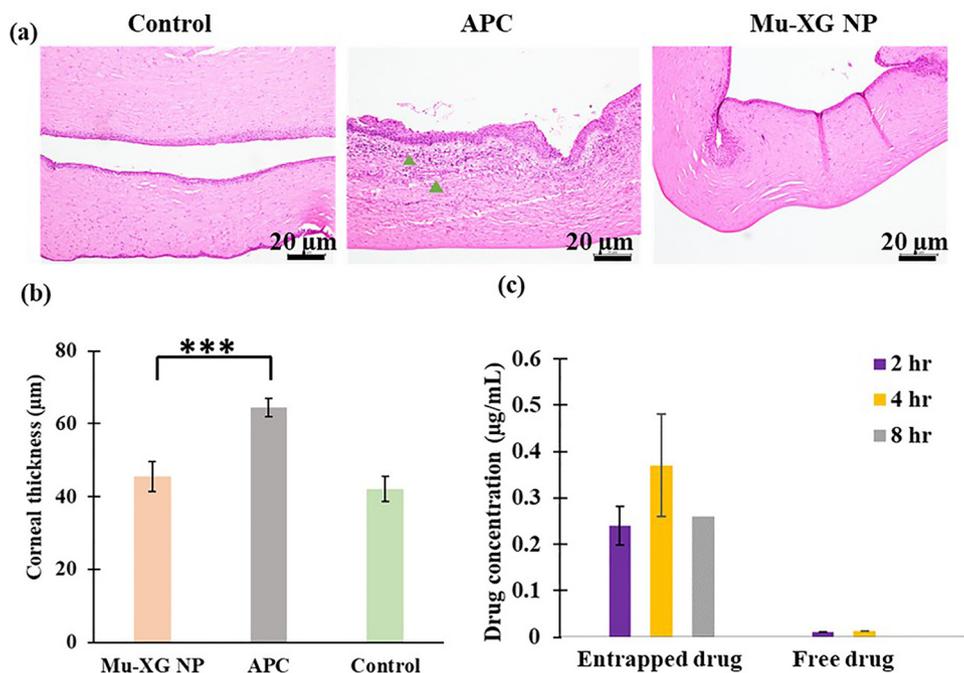
Fig. 8 Therapeutic effects of the CIP loaded Mu-XG NP and commercially available CIP eye drop in preventing eye infection. (a) H&E staining of the healthy cornea, cornea treated with APC and mucin nanoparticle on day 7. Triangles (green) in the H&E staining indicate the presence of inflammatory cells (primarily neutrophils). (b) Total corneal thickness measured after seven days of treatment. Presence of neutrophils after treatment with APC makes the corneal stroma swollen, increasing its thickness, whereas bacterial infection treatment with the Mu-XG NP has been completed successfully within 7 days and the thickness returned to normal, matching the healthy cornea. The average thickness of a healthy cornea (~ 40 μm), provided as a reference to compare the inflammation-induced swelling with the post-treatment recovery. Significant differences are indicated by *** ($p < 0.001$). (c) *In vivo* comparative analysis of drug concentration between the free drug and the drug encapsulated in the nanocarrier within rabbit aqueous humor over time. Even after 8 h of instillation, a significant amount of ciprofloxacin is present in the aqueous humor when applied using a mucin nanocarrier.

the inflammation was cured within 3 days. Moreover, *in vivo* bacterial infection was treated within 7 days and the nanoformulation was as effective as the commercial equivalent product despite the absence of additional components in the formulation while providing enhanced bioavailability. These findings suggest the potential applicability of ciprofloxacin-loaded mucin nanoparticles under ocular inflammatory conditions, particularly those affecting the anterior segment. However, further experiments are needed for optimizing the total number of dosages. To further validate these findings, improve the formulation performance, and facilitate future clinical translation, more extensive animal trials and more in-depth analysis including immunohistochemistry, levels of TNF-α, and IL-6 in the aqueous humor by ELISA will be needed. This study demonstrates that drugs such as ciprofloxacin can be efficiently integrated into a mucin nanocarrier and administered for intended purposes. The successful development of mucin nanocarrier will open the gate towards the application of ocular disorders ranging from ocular surface diseases to the retinal issues requiring prolonged drug release.

Author contributions

Wahida Binte Naz Aurthy: conceptualization, methodology, visualization, investigation, formal analysis, data curation, writing – original draft, writing – reviewing and editing. Nondita Datta: visualization, investigation. Siew Yee Wong: investigation. Xu Li: resources. Asma Rahman: investigation. Md. Latiful Bari: investigation, resources. Ishtiaque Anwar: investigation, resources. M Tarik Arafat: conceptualization, writing – reviewing and editing, supervision, funding acquisition, resources, project administration.

Conflicts of interest

The authors declare no conflict of interest.

Data availability

Additional data will be available upon request.

Supplementary information (SI) can be found online. See DOI: https://doi.org/10.1039/d5ma01442e.

Acknowledgements

References

1 A. B. Sallam, K. A. Kirkland, R. Barry, M. K. Soliman, T. K. Ali and S. Lightman, A Review of Antimicrobial Therapy for Infectious Uveitis of the Posterior Segment, *Med. Hypothesis Discovery Innov. Ophthalmol.*, 2018, **7**, 140–155.

2 Y. Zhang, *et al.*, Incidence, prevalence, and risk factors of infectious uveitis and scleritis in the United States: A claims-based analysis, *PLoS One*, 2020, **15**, 1–16.

3 G. Wildner, R. Bansal, N. Ayyadurai, S. Thurau and S. Basu, Pathogenesis of Bacterial Uveitis, *Ocul. Immunol. Inflamm.*, 2023, **31**, 1396–1404.

4 M. A. Asghar, S. Tang, L. P. Wong, P. Yang and Q. Zhao, Infectious uveitis: a comprehensive systematic review of emerging trends and molecular pathogenesis using network analysis, *J. Ophthalmic Inflamm. Infect.*, 2024, **14**, 60.

5 J. DeDreu, *et al.*, Uveitis-mediated immune cell invasion through the extracellular matrix of the lens capsule, *FASEB J.*, 2022, **36**, e21995.

6 R. B. Richardson, E. A. Ainsbury, C. R. Prescott and F. J. Lovicu, Etiology of posterior subcapsular cataracts based on a review of risk factors including aging, diabetes, and ionizing radiation, *Int. J. Radiat. Biol.*, 2020, **96**, 1339–1361.

7 S. M. Llop and G. N. Papaliodis, Cataract Surgery Complications in Uveitis Patients: A Review Article, *Semin. Ophthalmol.*, 2018, **33**, 64–69.

8 M. Teweldemedhin, H. Gebreyesus, A. H. Atsbaha, S. W. Asgedom and M. Saravanan, Bacterial profile of ocular infections: A systematic review, *BMC Ophthalmol.*, 2017, **17**, 1–9.

9 C. D. Conrady and S. Yeh, A review of ocular drug delivery platforms and drugs for infectious and noninfectious uveitis: The past, present, and future, *Pharmaceutics*, 2021, **13**, 1224.

10 A. Khare, K. Grover, P. Pawar and I. Singh, Mucoadhesive polymers for enhancing retention in ocular drug delivery: A critical review, *Rev. Adhes. Adhes.*, 2014, **2**, 467–502.

11 T. H. Tsung, Y. H. Chen and D. W. Lu, Updates on Biodegradable Formulations for Ocular Drug Delivery, *Pharmaceutics*, 2023, **15**, 734.

12 D. D. Nguyen, L.-J. Luo, C.-J. Yang and J.-Y. Lai, Highly Retina-Permeating and Long-Acting Resveratrol/Metformin Nanotherapeutics for Enhanced Treatment of Macular Degeneration, *ACS Nano*, 2023, **17**, 168–183.

13 C. Yang, D. D. Nguyen and J. Lai, Poly (l-Histidine)-Mediated On-Demand Therapeutic Delivery of Roughened Ceria Nanocages for Treatment of Chemical Eye Injury, *Adv. Sci.*, 2023, **10**, 1–15.

14 A. Bhattacharjee, *et al.*, Novel drug delivery systems for ocular therapy: With special reference to liposomal ocular delivery, *Eur. J. Ophthalmol.*, 2019, **29**, 113–126.

15 A. J. Sivaram, P. Rajitha, S. Maya, R. Jayakumar and M. Sabitha, Nanogels for delivery, imaging and therapy. Wiley Interdiscip, *Rev. Nanomed. Nanobiotechnol.*, 2015, **7**, 509–533.

16 Y. Diebold, *et al.*, Ocular drug delivery by liposome-chitosan nanoparticle complexes (LCS-NP), *Biomaterials*, 2007, **28**, 1553–1564.

17 J. Alvarez-Trabado, Y. Diebold and A. Sanchez, Designing lipid nanoparticles for topical ocular drug delivery, *Int. J. Pharm.*, 2017, **532**, 204–217.

18 F. Li, *et al.*, Characterisation of 2-HP-β-cyclodextrin-PLGA nanoparticle complexes for potential use as ocular drug delivery vehicles, *Artif. cells, Nanomed. Biotechnol.*, 2019, **47**, 4097–4108.

19 X. Liu, *et al.*, Multifunctional Hydrogel Eye Drops for Synergistic Treatment of Ocular Inflammatory Disease, *ACS Nano*, 2023, **17**, 25377–25390.

20 B. Unnikrishnan, J.-Y. Lai, A. Anand, C.-C. Huang and H.-T. Chang, Tiny tools, big vision: A minireview on carbonized nanomaterials in ophthalmology, *J. Controlled Release*, 2025, **388**, 114396.

21 R. Agarwal, *et al.*, Liposomes in topical ophthalmic drug delivery: an update, *Drug Delivery*, 2016, **23**, 1075–1091.

22 T. Nakamura, *et al.*, JBP485 promotes tear and mucin secretion in ocular surface epithelia, *Sci. Rep.*, 2015, **5**, 1–11.

23 F. Mantelli and P. Argüeso, Functions of ocular surface mucins in health and disease, *Curr. Opin. Allergy Clin. Immunol.*, 2008, **8**, 477–483.

24 J. S. Lee, J. W. Suh, E. S. Kim and H. G. Lee, Preparation and Characterization of Mucoadhesive Nanoparticles for Enhancing Cellular Uptake of Coenzyme Q10, *J. Agric. Food Chem.*, 2017, **65**, 8930–8937.

25 T. Irimia, M. V. Ghica, L. Popa, V. Anuta, A.-L. Arsene and C.-E. Dinu-Pîrvu, Strategies for improving ocular drug bioavailability and corneal wound healing with chitosan-based delivery systems, *Polymers*, 2018, **10**, 1221.

26 Y. Almoshari, Osmotic Pump Drug Delivery Systems—A Comprehensive Review, *Pharmaceuticals*, 2022, **15**, 1430.

27 S. H. Lim, *et al.*, Mucin coated protein-polyphenol microcarriers for daidzein delivery, *Food Funct.*, 2024, **15**, 2645–2654.

28 A. Dedinaite, M. Lundin, L. Macakova and T. Auletta, Mucin-chitosan complexes at the solid-liquid interface: Multilayer formation and stability in surfactant solutions, *Langmuir*, 2005, **21**, 9502–9509.

29 K. Shirai and S. Saika, Ocular surface mucins and local inflammation-Studies in genetically modified mouse lines, *BMC Ophthalmol.*, 2015, **15**, 47–65.

30 R. R. Hodges and D. A. Dartt, Tear film mucins: front line defenders of the ocular surface; comparison with airway and gastrointestinal tract mucins, *Exp. Eye Res.*, 2013, **117**, 62–78.

31 C. Kimna, T. M. Lutz and O. Lieleg, Fabrication and Characterization of Mucin Nanoparticles for Drug Delivery Applications, *Methods Mol. Biol.*, 2024, **2763**, 383–394.

32 K. Nissen, J. S. Jørgensen, J. C. Nørregaard, A. Storr-Paulsen and D. Bach-Holm, The effect of orally administered glycerol on anterior chamber depth during cataract surgery in eyes with narrow anterior chambers, *Acta Ophthalmol.*, 2021, **99**, 156–159.

33 E. Szél, *et al.*, Anti-irritant and anti-inflammatory effects of glycerol and xylitol in sodium lauryl sulphate-induced acute irritation, *J. Eur. Acad. Dermatol. Venereol.*, 2015, **29**, 2333–2341.

34 S. Srinivasan and R. Williams, Propylene Glycol and Hydroxypropyl Guar Nanoemulsion-Safe and Effective Lubricant Eye Drops in the Management of Dry Eye Disease, *Clin. Ophthalmol.*, 2022, **16**, 3311–3326.

35 M. Jadav, D. Pooja, D. J. Adams and H. Kulhari, Advances in Xanthan Gum-Based Systems for the Delivery of Therapeutic Agents, *Pharmaceutics*, 2023, **15**, 1–27.

36 B. Katzbauer, Properties and applications of xanthan gum, *Polym. Degrad. Stab.*, 1998, **59**, 81–84.

37 N. Datta, T. Jinan, S. Y. Wong, S. Chakravarty, X. Li, I. Anwar and M. T. Arafat, Self-assembled sodium alginate polymannuronate nanoparticles for synergistic treatment of ophthalmic infection and inflammation: Preparation optimization and *in vitro/vivo* evaluation, *Int. J. Biol. Macromol.*, 2024, **262**, 130038.

38 S. Pedroso-santana, *Ionotropic gelation method in the synthesis of nanoparticles/microparticles for biomedical purposes.* 2020, DOI: 10.1002/pi.5970.

39 E. Martins, D. Poncelet, R. C. Rodrigues and D. Renard, Oil encapsulation in core–shell alginate capsules by inverse gelation II: comparison between dripping techniques using W/O or O/W emulsions, *J. Microencapsul.*, 2017, **34**, 522–534.

40 M. A. Patel, M. H. H. AbouGhaly, J. V. Schryer-Praga and K. Chadwick, The effect of ionotropic gelation residence time on alginate cross-linking and properties, *Carbohydr. Polym.*, 2017, **155**, 362–371.

41 K. Joyner, D. Song, R. F. Hawkins, R. D. Silcott and G. A. Duncan, Designing viscoelastic mucin-based hydrogels, *bioRxiv*, preprint, 656801, 2019, DOI: 10.1101/656801.

42 E. Szliszka, *et al.*, Ionotropic Gerlation of Chitosan Flat Structures and Potential Applications, *Molecules*, 2009, **14**, 738–754.

43 K. Kobra, S. Y. Wong, M. A. J. Mazumder, X. Li and M. T. Arafat, Xanthan and gum acacia modified olive oil based nanoemulsion as a controlled delivery vehicle for topical formulations, *Int. J. Biol. Macromol.*, 2023, **253**, 126868.

44 S. I. Swapnil, M. T. H. Shoudho, A. Rahman, T. Ahmed and M. T. Arafat, DOTAGEL: a hydrogen and amide bonded, gelatin based, tunable, antibacterial, and high strength adhesive synthesized in an unoxidized environment, *J. Mater. Chem. B*, 2024, **12**, 11025–11041.

45 P. C. Agu, *et al.*, Molecular docking as a tool for the discovery of molecular targets of nutraceuticals in diseases management, *Sci. Rep.*, 2023, **13**, 1–18.

46 P. Xie, Y. Gao, C. Wu, X. Li and Y. Yang, The inhibitory mechanism of echinacoside against Staphylococcus aureus Ser/Thr phosphatase Stp1 by virtual screening and molecular modeling, *J. Mol. Model.*, 2023, **29**, 1–11.

47 F. Akhtar, K. Kobra, S. Yee, X. Li and M. T. Arafat, Glycerol crosslinked vitamin E loaded xanthan gum and gellan gum nanoemulgels for topical management of dry skin, *Int. J. Biol. Macromol.*, 2025, **333**, 148769.

48 S. Privitera, G. Manetto, S. Pascuzzi, D. Pessina and E. Cerruto, Drop Size Measurement Techniques for Agricultural Sprays: A State-of-The-Art Review, *Agronomy*, 2023, **13**, 678.

49 B. Devrim, A. Bozkir and K. Canefe, Formulation and evaluation of reconstitutable suspensions containing ibuprofen-loaded Eudragit microspheres, *Acta Pol. Pharm. Drug Res.*, 2011, **68**, 593–599.

50 K. Shah, S. K. Shrivastava and P. Mishra, Formulation and evaluation of suspensions: mefenamic acid prodrugs, *Pak. J. Pharm. Sci.*, 2014, **27**, 917–923.

51 A. M. da Nóbrega, E. N. Alves, R. de Farias Presgrave, R. N. Costa and I. F. Delgado, Determination of eye irritation potential of low-irritant products: Comparison of in vitro results with the in vivo Draize rabbit test, *Brazilian Arch. Biol. Technol.*, 2012, **55**, 381–388.

52 W. Zhang, *et al.*, Nanostructured lipid carrier surface modified with Eudragit RS 100 and its potential ophthalmic functions, *Int. J. Nanomed.*, 2014, **9**, 4305–4315.

53 G. Jiang, *et al.*, Plga nanoparticle platform for trans-ocular barrier to enhance drug delivery: A comparative study based on the application of oligosaccharides in the outer membrane of carriers, *Int. J. Nanomed.*, 2020, **15**, 9373–9387.

54 L. Jamieson, D. Meckoll-Brinck and N. Keller, Characterized and predictable rabbit uveitis model for antiinflammatory drug screening, *J. Pharmacol. Methods*, 1989, **21**, 329–338.

55 T. Wada, H. Jensen and S. M. Whitcup, Treatment of rabbit corneal infections with ophthalmic gatifloxacin: a concentration dependence study, *Adv. Ther.*, 2004, **21**(1), 1–12.

56 W. Lin, Q. Tan and D. Lin, Treatment of severe acute bacterial keratitis in rabbits using continuous topical ocular instillation with norvancomycin, *Drug Des., Dev. Ther.*, 2021, **15**, 617–628.

57 D. J. Thornton, C. Sharpe and C. Ridley, Intracellular processing of human secreted polymeric airway mucin, *Ann. Am. Thorac. Soc.*, 2018, **15**, S154–S158.

58 G. Petrou and T. Crouzier, Mucins as multifunctional building blocks of biomaterials, *Biomater. Sci.*, 2018, **6**, 2282–2297.

59 Z. Németh, I. Csóka, R. Semnani Jazani, B. Sipos, H. Haspel, G. Kozma, Z. Kónya and D. G. Dobó, Quality by design-driven zeta potential optimisation study of liposomes with charge imparting membrane additives, *Pharmaceutics*, 2022, **14**, 1798.

60 H. Daemi and M. Barikani, Synthesis and characterization of calcium alginate nanoparticles, sodium homopolymannuronate salt and its calcium nanoparticles, *Sci. Iran.*, 2012, **19**, 2023–2028.

61 M. Abyadeh, A. A. Karimi Zarchi, M. A. Faramarzi and A. Amani, Evaluation of factors affecting size and size distribution of chitosan-electrosprayed nanoparticles, *Avicenna J. Med. Biotechnol.*, 2017, **9**, 126–132.

62 C. Pan, *et al.*, Study on the relationship between cross-linking degree and properties of TPP crosslinked chitosan nanoparticles, *Carbohydr. Polym.*, 2020, **241**, 116349.

63 E. F. Ribeiro, *et al.*, Chitosan and crosslinked chitosan nanoparticles: Synthesis, characterization and their role as Pickering emulsifiers, *Carbohydr. Polym.*, 2020, **250**, 116878.

64 D. Saha and S. Bhattacharya, Hydrocolloids as thickening and gelling agents in food: A critical review, *J. Food Sci. Technol.*, 2010, **47**, 587–597.

65 D. M. Walden, M. Khotimchenko, H. Hou, K. Chakravarty and J. Varshney, Effects of magnesium, calcium, and aluminum chelation on fluoroquinolone absorption rate and bioavailability: A computational study, *Pharmaceutics*, 2021, **13**, 594.

66 J. Yu, *et al.*, Multiple roles of Ca2+ in the interaction of ciprofloxacin with activated sludge: Spectroscopic investigations of extracellular polymeric substances, *Sci. Total Environ.*, 2021, **751**, 142246.

67 N. Watcharadulyarat, M. Rattanatayarom, N. Ruangsawasdi and N. Patikarnmonthon, PEG–PLGA nanoparticles for encapsulating ciprofloxacin, *Sci. Rep.*, 2023, **13**, 1–11.

68 Z. Sobhani, S. M. Samani, H. Montaseri and E. Khezri, Nanoparticles of chitosan loaded ciprofloxacin: Fabrication and antimicrobial activity, *Adv. Pharm. Bull.*, 2017, **7**, 427–432.

69 W. Kapadia, *et al.*, Shear-Thinning and Temperature-Dependent Viscosity Relationships of Contemporary Ocular Lubricants, *Transl. Vis. Sci. Technol.*, 2022, **11**, 1–10.

70 P. Aragona, P. A. Simmons, H. Wang and T. Wang, Physicochemical properties of hyaluronic acid–based lubricant eye drops, *Transl. Vis. Sci. Technol.*, 2019, **8**(6), 2.

71 F. A. Che Arif, M. R. Hilmi, K. Mohd Kamal and M. H. Ithnin, Evaluation of 18 artificial tears based on viscosity and pH, *Malaysian J. Ophthalmol.*, 2020, **2**, 96–111.

72 S. Kummar, N. R. Dull, S. Helsper and M. W. Liberatore, Effect of shear rate, temperature, and salts on the viscosity and viscoelasticity of semi-dilute and entangled xanthan gum, *J. Appl. Polym. Sci.*, 2024, 1–10, DOI: 10.1002/app.56372.

73 S. Y. Khan, M. Yusuf and N. Sardar, Studies on Rheological Behavior of Xanthan Gum Solutions in Presence of Additives, *Pet. Petrochem. Eng. J.*, 2018, **2**, 1–7.

74 F. Lallemand, P. Daull, S. Benita, R. Buggage and J.-S. Garrigue, Successfully Improving Ocular Drug Delivery Using the Cationic Nanoemulsion, Novasorb, *J. Drug Delivery*, 2012, 1–16.

75 T. Quinten, *et al.*, Sustained-release and swelling characteristics of xanthan gum/ethylcellulose-based injection moulded matrix tablets: In vitro and in vivo evaluation, *J. Pharm. Sci.*, 2011, **100**, 2858–2870.

76 A. Aranega and H. Boulaiz, Cellular and Molecular Biology: Foreword, *Cell. Mol. Biol.*, 2005, **51**, 1.

77 H. G. Merkus, *Particulate Products*, 19, 253–272 (2014).

78 S. Mahmood, U. K. Mandal, B. Chatterjee and M. Taher, Advanced characterizations of nanoparticles for drug delivery: Investigating their properties through the techniques used in their evaluations, *Nanotechnol. Rev.*, 2017, **6**, 355–372.

79 S. H. Hussein-Al-Ali, *et al.*, Preparation and characterisation of ciprofloxacin-loaded silver nanoparticles for drug delivery, *IET Nanobiotechnol.*, 2022, **16**, 92–101.

80 N. Kamaly, B. Yameen, J. Wu and O. C. Farokhzad, Nanoparticles: Mechanisms of Controlling Drug Release, *Chem. Rev.*, 2016, **116**, 2602–2663.

81 N. S. Heredia, *et al.*, Comparative statistical analysis of the release kinetics models for nanoprecipitated drug delivery systems based on poly(lactic-*co*-glycolic acid), *PLoS One*, 2022, **17**, 1–28.

82 S. Dash, P. N. Murthy, L. Nath and P. Chowdhury, Kinetic modeling on drug release from controlled drug delivery systems, *Acta Pol. Pharm. Drug Res.*, 2010, **67**, 217–223.

83 Y. Fan, M. Lüchow, Y. Zhang, J. Lin, L. Fortuin, S. Mohanty, A. Brauner and M. Malkoch, Nanogel Encapsulated Hydrogels As Advanced Wound Dressings for the Controlled Delivery of Antibiotics, *Adv. Funct. Mater.*, 2021, **31**, 2006453.

84 J. Ferez-Vilar and R. L. Hill, The structure and assembly of secreted mucins, *J. Biol. Chem.*, 1999, **274**, 31751–31754.

85 A. M. Wu, G. Csako and A. Herp, Structure, biosynthesis, and function of salivary mucins, *Mol. Cell. Biochem.*, 1994, **137**, 39–55.

86 L. Wang, *et al.*, Injectable hyaluronic acid hydrogel loaded with BMSC and NGF for traumatic brain injury treatment, *Mater. Today Bio*, 2022, **13**, 100201.

87 P. S. Taskar, A. Patil, P. Lakhani, E. Ashour, W. Gul, M. A. ElSohly, B. Murphy and S. Majumdar, Δ^9-Tetrahydrocannabinol Derivative-Loaded Nanoformulation Lowers Intraocular Pressure in Normotensive Rabbits, *Transl. Vis. Sci. Technol.*, 2019, **8**(5), 15.

88 E. Szél, *et al.*, Anti-irritant and anti-inflammatory effects of glycerol and xylitol in sodium lauryl sulphate-induced acute irritation, *J. Eur. Acad. Dermatology Venereol.*, 2015, **29**, 2333–2341.

89 M. C. Callegan, M. Engelbert, D. W. P. Ii, B. D. Jett and M. S. Gilmore, Bacterial Endophthalmitis: Epidemiology, Therapeutics, and Bacterium-Host Interactions, *Clin. Microbiol. Rev.*, 2002, **15**, 111–124.

90 M. Troisi, S. D. Prete, S. Troisi, M. V. Turco, M. Turco, A. D. Prete, G. Alessandro, G. Antonio and D. Marasco, Utility of scanning electron microscopy (SEM) for suspected microbial keratoconjunctivitis unresponsive to broad-spectrum antibiotic therapy, *J. Clin. Stud. Med. Case Rep.*, 2023, **10**(1), 155.

91 S. Das, S. Singh and A. Kumar, Bacterial Burden Declines But Neutrophil Infiltration and Ocular Tissue Damage Persist in Experimental Staphylococcus epidermidis Endophthalmitis, *Front. Cell. Infect. Microbiol.*, 2021, **11**, 1–14.